*Mineralogical Magazine, February 2009, Vol. 73(1), pp. 59–82*

# The role of fractional crystallization and late-stage peralkaline melt segregation in the mineralogical evolution of Cenozoic nephelinites/phonolites from Saghro (SE Morocco)

J. Berger[1,2,3,*], N. Ennih[4], J.-C. C. Mercier[3,5], J.-P. Liégeois[1] and D. Demaiffe[2]

[1] Section de Géologie Isotopique, Musée Royal de l'Afrique Centrale, 3080 Tervuren, Belgium
[2] Laboratoire de Géochimie Isotopique et Géodynamique Chimique, CP160/02, Université Libre de Bruxelles (U.L.B.), 1050 Brussels, Belgium
[3] UMR CNRS 6250 "LIENSs", Université de La Rochelle, ILE, 2 rue Olympe de Gouges 17042 La Rochelle Cedex-1, France
[4] Laboratoire de Géodynamique, Université d'El Jadida, BP20, 24000 El Jadida, Morocco
[5] UMR CNRS 6112 "Planétologie et Géodynamique (LPGN)", Université de Nantes, BP 92205, 2 rue de la Houssinière, 44322 Nantes, France

[*Received 17 June 2008; Accepted 26 February 2009*]

**ABSTRACT**

The Saghro Cenozoic lavas form a bimodal suite of nephelinites (with carbonatite xenoliths) and phonolites emplaced in the Anti-Atlas belt of Morocco. Despite the paucity of samples with intermediate composition between the two main types of lava (only one phonotephrite flow is reported in this area), whole-rock major element modelling shows that the two main lithologies can be linked by fractional crystallization. The most primitive modelled cumulates are calcite-bearing olivine clinopyroxenites, whereas the final stages of differentiation are characterized by the formation of nepheline-syenite cumulates. This evolution trend is classically observed in plutonic alkaline massifs associated with carbonatites. Late-stage evolution is responsible for the crystallization of hainite- and delhayelite-bearing microdomains, for the transformation of aegirine-augite into aegirine (or augite into aegirine-augite), and for the crystallization of lorenzenite and a eudialyte-group mineral as replacement products of titanite. These phases were probably formed, either by crystallization from late residual peralkaline melts, or by reaction of pre-existing minerals with such melt, or hydrothermal peralkaline fluid.

**Keywords:** nephelinite, peralkaline phonolite, carbonatite, Daly gap, hainite, fractional-crystallization modelling, Mio-Pliocene volcanism.

## Introduction

The mineralogy of peralkaline plutonic and volcanic suites (rocks with the molar ratio (Na+K)/Al >1) is extremely diverse. The uncommon, but well documented, intrusions of peralkaline nepheline syenite referred to as 'agpaitic' (nephelinite-syenites characterized by the presence of *REE*, Zr, Nb and volatile-rich minerals, Sørensen, 1997), i.e. the Lovozero and Khibina massifs in the Kola peninsula, Russia, (Kogarko *et al*., 1995), the Ilimaussaq intrusion, Greenland, (Larsen and Sørensen, 1987), the Mont Saint-Hilaire massif, Quebec, (Currie *et al*., 1986), Poços de Caldas, Brazil (Ulbrich *et al*., 2005) and the Los Islands, Guinea, (Moreau *et al*., 1996), are known for their great variety of unusual mineral phases (more than 500 species, Moreau *et al*., 1996). These minerals are generally rich in Na, volatiles (F, Cl) and elements (mainly the HFSE and *REE*) usually only present as traces in minerals from other less alkaline or subalkaline

* E-mail: juberger@ulb.ac.be
DOI: 10.1180/minmag.2009.073.1.59

magmatic bodies. Accordingly, peralkaline massifs have been mined locally for rare elements (Zr, *REE*, Nb, Ta, U) and they are sometimes associated with carbonatites. Crystallization of peralkaline rocks is also known to occur over a wide temperature interval and sometimes down to unusually low temperatures (solidus near 400ºC; Kogarko and Romanchev, 1977; Sørensen, 1997; Marks and Markl, 2003) which, together with the unusual chemistry of the melts and/or late hydrothermal solutions, permit the crystallization of numerous uncommon mineral species. The existence of trapped interstitial silicate melt, rich in Na-F-Zr in syenites, further demonstrates that fractional crystallization can actually lead to the production of melts able to crystallize these rare minerals (Wolff and Toney, 1993), but the transformation of magmatic phases by reaction with fluids exsolved from the crystallizing melt is also documented as an alternative process for some species (Schonenberger *et al*., 2006; Mitchell and Liferovich, 2006). By contrast, peralkaline phonolites, the volcanic equivalent of plutonic nepheline-syenites, show a less varied mineralogy which probably reflects their greater cooling rate in superficial lava flows.

The Cenozoic Saghro phonolites and nephelinites described in this paper constitute a poorly-known occurrence of strongly alkaline lavas characterized by a variable and complex mineralogy and by the occurrence of rare carbonatitic xenoliths (Ibhi, 2000; Ibhi *et al*., 2002). This paper presents a detailed study of the lava suite based on major-element mineral and whole-rock data and provides evidence for a fractional crystallization mechanism linking the nephelinites to the phonolites despite the paucity of intermediate lavas at the surface. The formation of rare, late mineral phases in the phonolites is also attributed to late-magmatic and/or subsolidus-hydrothermal processes.

## Geological setting

The Cenozoic lavas from Saghro, first recognized by de Sitter *et al* (1952), are located on the northern edge of the West African Craton (WAC), in the Anti-Atlas belt (Fig. 1). The lavas erupted in two periods: 10−6 Ma for the nephelinites and phonolites in southern Saghro and 5−3 Ma for the nephelinites cropping out in the northernmost part of eastern Saghro (Berrahma *et al*., 1993). The

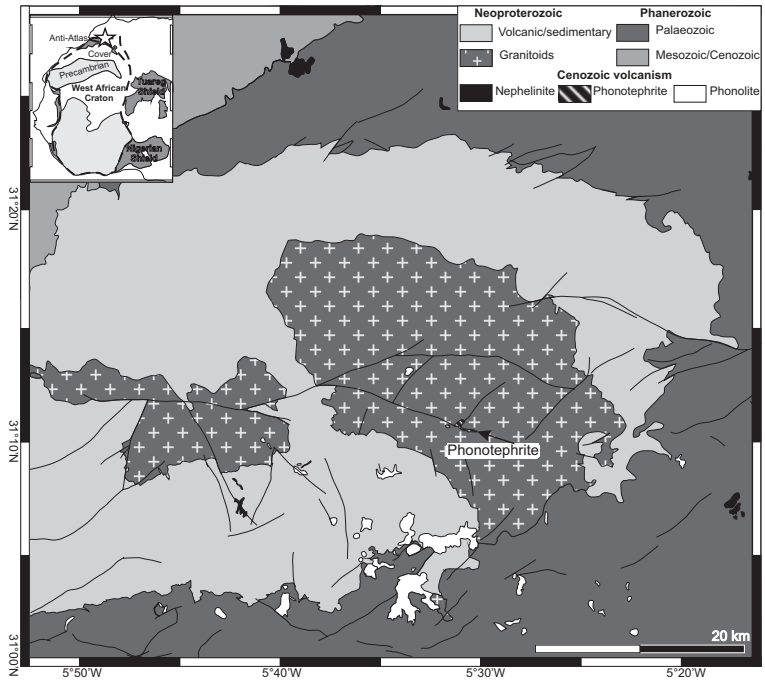


FIG. 1. Geological sketch of westernmost Saghro showing the location of the Cenozoic nephelinites, phonotephrites and phonolites. The inset shows the location of the Saghro inlier (star) in West Africa.

cause of the volcanism remains uncertain. Ibhi (2000) proposed that a mantle plume was at the origin of this magmatism by analogy with the Canary Islands. Liégeois *et al*. (2005) included the Saghro volcanism in the West African Cenozoic volcanism as a whole and proposed that it has been enhanced by reactivation of the Pan-African structures affecting the northern boundary of the West African craton during the Africa-Europe convergence. New data concerning the Cenozoic tectonics and sedimentological record within the Atlasic domain show that the period of Cenozoic volcanic activity in Saghro (and in Morocco as a whole) closely corresponds to major episodes of tectonic activity in the Atlasic belts and adjacent areas (Malusa *et al*., 2007; Tesón and Teixell, 2008). This suggests a tectonic control of the volcanism, related to the building of the Atlas Mountains, rather than a mantle plume model.

The volcanic deposits are of three main types: lava flows, phonolitic domes and pyroclastic deposits. Nephelinites are always present as thin lava flows (<15 m thick) located at high topographic levels. They are generally underlain by thin strata (<1 m) of pyroclastic tuffs, locally rich in megacrysts and xenoliths (Ibhi, 2000). Phonolites are present either as thick flows (<50 m thick) lying on present day topographic highs or as domes ranging from 500 m to 1 km in diameter. Only one prismated flow of phonotephrite occurs in the Saghro area. It is strongly eroded and the original magmatic structures cannot be observed. Pyroclastic deposits are mainly phonolitic tuffs and volcanic breccias containing volcanic and basement rock pebbles.

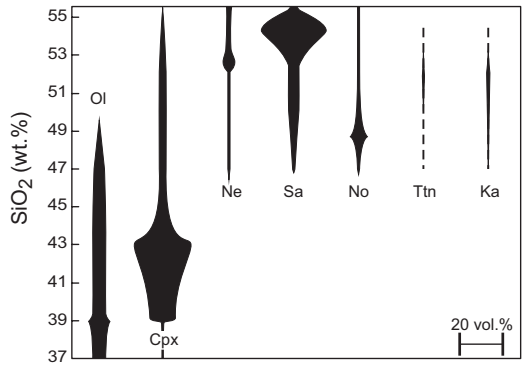


FIG. 2. Evolution of the modal proportions of the major and minor phenocryst phases as a function of whole-rock silica content. From left to right, the abbreviations stand for olivine, clinopyroxene, nepheline, sanidine, nosean, titanite, kaersutite.

## Petrographical description

### *Nephelinites*

The nephelinites are holocrystalline with a groundmass dominated by clinopyroxene and nepheline with minor amounts of Ti-magnetite, apatite and late-magmatic perovskite developing around the Ti-magnetite crystals. Nepheline is interstitial between the other groundmass phases, being a late-crystallizing phase relative to clinopyroxene, apatite and Ti-magnetite. Different types of nephelinite were distinguished on the basis of the abundance of the main phenocrysts (Fig. 2).

#### *Olivine nephelinites*

Olivine nephelinites ($SiO_2$ <39 wt.%) are dominated by euhedral to subhedral olivine phenocrysts occurring either as microphenocrysts (<0.1 cm; sample TAF7) or large phenocrysts (up to 0.5 cm; sample FN4). Inclusions of calcite associated with apatite, nepheline and spinel are common in the core of olivine from TAF7. Pyroxene phenocrysts are present in small proportions (<2 vol.%); they have a light-brown-coloured core surrounded by a thin rim of brown augite, similar in optical properties to the augite in the groundmass. One sample (FN3) is characterized by the presence of resorbed green cores in the pyroxenes (Fig. 3*a*; see Berger *et al*., 2008). Another sample (TL6) shows minor amounts (<1 vol.%) of partly altered melilite in the groundmass (Fig. 3*b*), dominantly anhedral olivine and pyroxene with a light-brown coloured core rich in fluid inclusions, and a thin external rim of brown augite.

#### *Pyroxene nephelinites*

Pyroxene nephelinites (FS5, TAB3; $SiO_2$ 39–46 wt.%) are dominated by phenocrysts of Ti-augite with minor amounts of olivine. Three types of pyroxene phenocrysts are present: (1) augite with a green resorbed core surrounded by a brown mantle; (2) pyroxene with a dark brown resorbed core and a light-brown mantle and (3) small light-brown euhedral phenocrysts. A detailed study of the pyroxene compositions, textures and crystallization conditions is given in Berger *et al*. (2008). Perovskite is abundant in the groundmass of these samples: it is sometimes

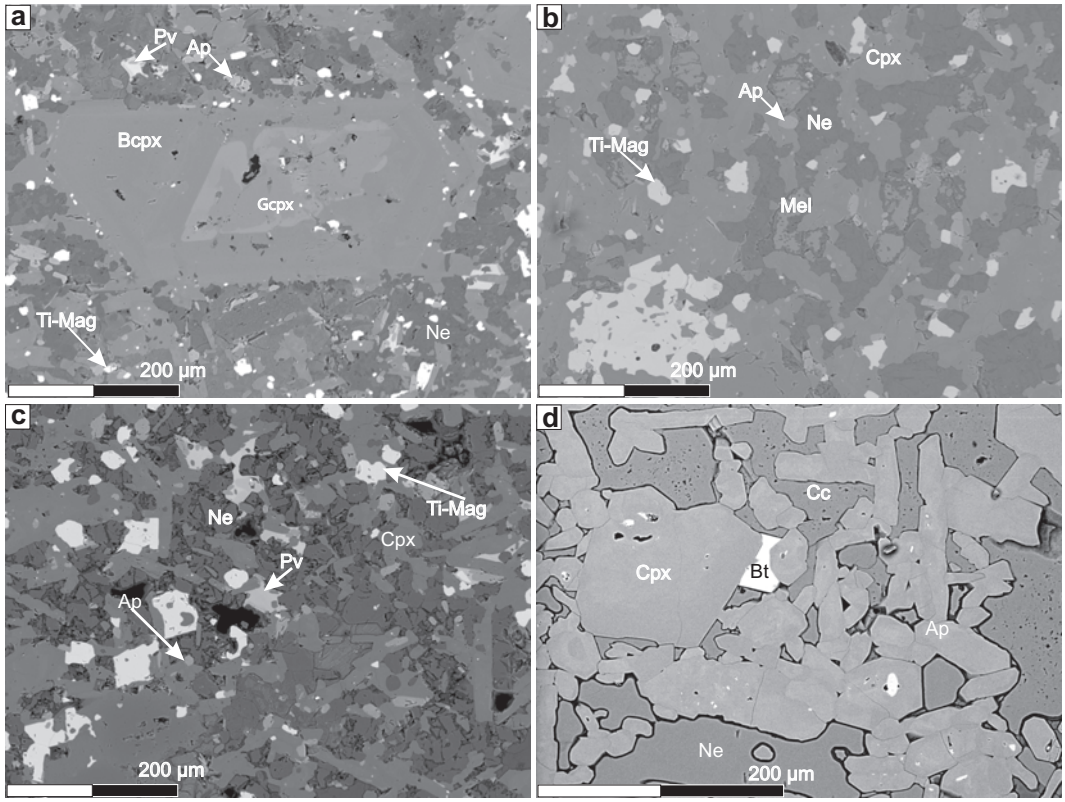


FIG. 3. BSE images showing some of the mineralogical features in nephelinites. (*a*) Green core, Na-Fe rich clinopyroxene (Gcpx) surrounded by a Ca-Mg rich-brown mantle (Bcpx). (*b*) Altered melilite (Mel) in the groundmass of a melilite-olivine nephelinite. (*c*) Perovskite (Pv) in the groundmass of a pyroxene-nephelinite; note that perovskite is rimming Ti-magnetite on the left of the BSE image. (*d*) Calcite (Cc) interstitial to euhedral pyroxenes (Cpx) and containing Ba-rich biotite (Bt) and apatite (Ap).

found in association with Ti-magnetite but it may also occur independently (Fig. 3*c*). In our samples, carbonates are present either as fine-grained material in association with euhedral clinopyroxene, apatite and Ba-rich biotite (Fig. 3*d*) or as inclusions within the olivine of an olivine nephelinite. In the latter case, the carbonate inclusions are associated with a few small grains of Cr-bearing spinel and apatite.

### *Phonotephrite*

The phonotephrite (AS1; $SiO_2$ ~47 wt.%) has a groundmass comprising sanidine, green pyroxene, nepheline, Ti-magnetite and minor apatite. Numerous phenocrysts of strongly-to-totally resorbed olivine are present as well as micro-phenocrysts of light-green and brown pyroxene sometimes showing a resorbed green core (Fig. 4*a*). Phenocrysts of nosean, nepheline, brown amphibole and brown mica are also observed. These last two phases are always surrounded by fine-grained coronas of augite, Ti-magnetite and sanidine. This sample is also remarkable for the abundance of fine-grained pyroxenite xenoliths and subvolcanic-to-volcanic xenoliths made of pyroxene nephelinite containing small amounts of brown mica.

### *Phonolites*

All the phonolites share two common features: (1) a strong magmatic fabric illustrated by the preferred orientation of the sanidine crystals and/or of the aegirine-augite needles (C/S fabrics are locally developed within some lava flows);

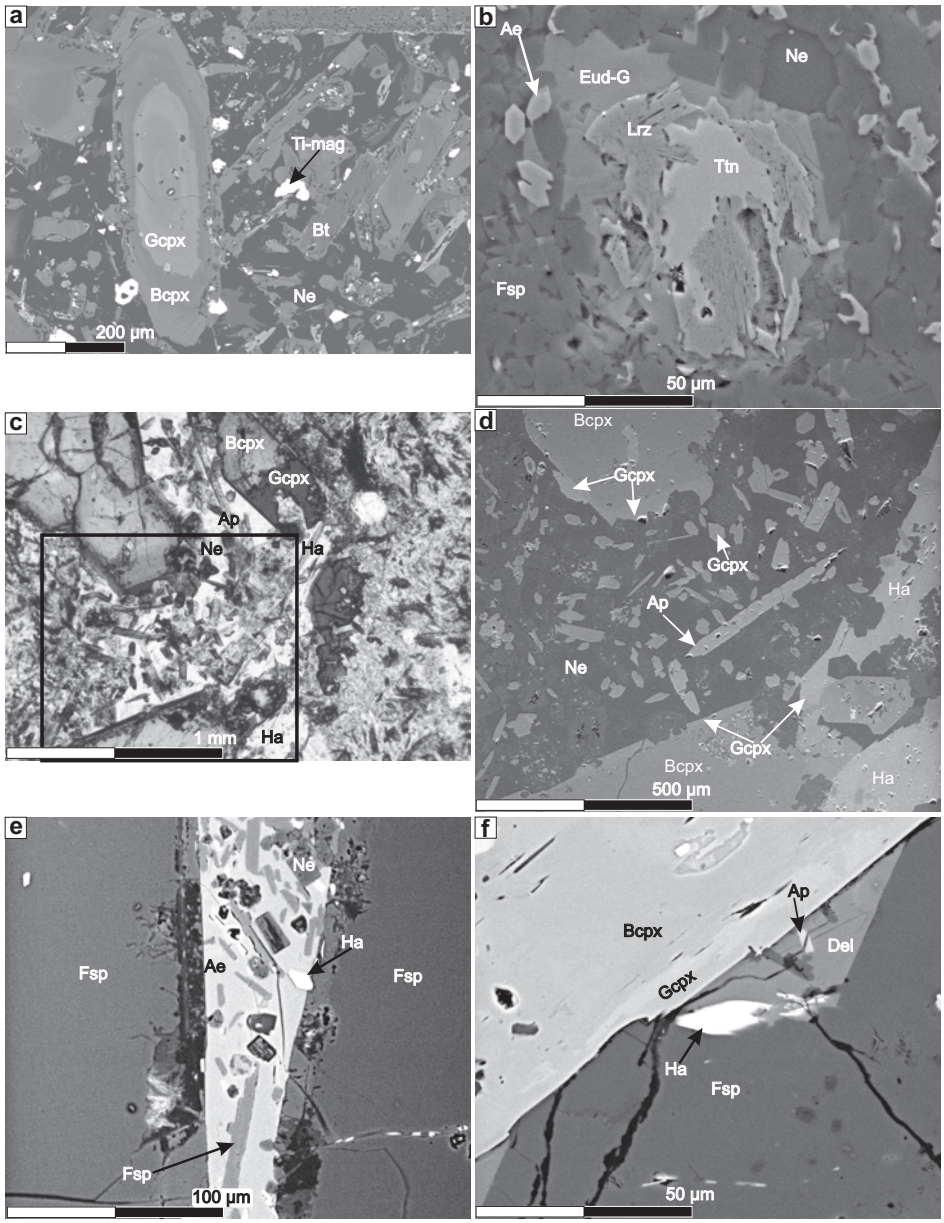


FIG. 4. BSE and optical images of phonotephrite and phonolites. (*a*) Clinopyroxene with a green core (Gcpx) and a brown rim (Bcpx) in the phonotephrite. (*b*) Corroded titanite (Ttn) partly surrounded by lorenzenite (Lrz) and an unidentified mineral (Eud-G, close to eudialyte-group minerals, see text) in a peralkaline phonolite. (*c*) An interstitial hainite-bearing microdomain in a peralkaline phonolite. Note that at the contact with the peralkaline domain, a green pyroxene (Gcpx) rim has crystallized at the border of brown augite (Bcpx) phenocrysts and that some phenocrysts have been partly transformed into green aegirine-augite (Gcpx); the inset shows the location of the next BSE image. (*d*) BSE image of the same interstitial domain showing the precise location of hainite (Ha) and needle-like apatite (Ap). (*e*) Aegirine (Ae) interstitial to the alkali feldspar (Fsp) phenocrysts in a phonolite; it contains small euhedral inclusions of sanidine, nepheline, apatite and hainite. (*f*) A small microdomain between a feldspar phenocryst and an augite phenocryst showing delhayelite (Del) with euhedral inclusions of sanidine, apatite and hainite.

(2) sanidine is the dominant felsic mineral over nepheline. The phonolites fall into three groups according to chemistry and mode, two being represented in lava flows and the third in lava domes.

Samples from the phonolite lava flows have a groundmass comprising sanidine, nepheline and aegirine-augite with minor titanite, apatite, Fe-Ti oxides and aegirine. The phenocryst assemblage is the same for most samples and consists of sanidine, nepheline, aegerine-augite and titanite with minor nosean.

Sanidine-poor lava-flow phonolites ($SiO_2$ 47–52 wt.%; AZLOU1, MIG2, OUL3, TAB7, TG4, TO1) have a small proportion of phenocrysts (<10 vol.%) with glomerocrysts of euhedral nepheline, brown and green unzoned clinopyroxene phenocrysts with minor titanite, resorbed amphibole and sanidine phenocrysts. One of these samples (TG4) is characterized by the presence of strongly-resorbed olivine phenocrysts and trace amounts of nosean. Samples OUL3 and TO1 (with a peralkalinity index <1; see below) have the greatest content of nepheline phenocrysts (3–4 vol.%) with a very low feldspar content (<2 vol.%). The titanite of phonolite MIG2 is resorbed and partly replaced by an optically unidentifiable mineral that has been identified, using SEM-EDS analysis, as lorenzenite ($Na_2Ti_2Si_2O_9$) (Fig. 4*b*). An external corona of a poorly-identified mineral, close to the eudialyte group of minerals in terms of stoichiometry (see mineral chemistry section), surrounds the lorenzenite in this sample.

Sanidine-rich lava-flow phonolites ($SiO_2$ 53–55 wt.%; TIM1, SAR3, BAG2) contain up to 30 vol.% of sanidine phenocrysts as well as brown and green clinopyroxene phenocrysts. Euhedral nepheline is present together with titanite but in minor proportions (<1 vol.%). In TIM1 and BAG2, small microdomains (<1 vol.% of the whole thin section) or patches consisting of nepheline, sanidine, needle-like apatite, hainite ($Na_4Ca_8(Ti,Zr,Mn,Fe)_3Si_8O_{28}F_8$) and aegirine have been observed in interstitial position between clinopyroxene and feldspar phenocrysts (Fig. 4*c–f*). At the contact with these microdomains, the brown augite phenocrysts are transformed into a green aegirine-augite (Fig. 4*c–d*). Small delhayelite-group minerals have been observed between clinopyroxene and sanidine phenocrysts (Fig. 4*f*); they also contain inclusions of sanidine, apatite and hainite. One lava from this group (TAB1) has an unusual phenocryst assemblage rich in nosean phenocrysts with minor resorbed anhedral sanidine and olivine.

### *Si-rich phonolites*

Si-rich phonolites ($SiO_2$ >55 wt.%; IK01, ELB6) occur exclusively as lava domes. Sanidine, nepheline, aegirine and Fe-Ti oxides are present in the groundmass and as phenocrysts. The total phenocryst content is low (<10 vol.%).

### *Cognate xenolith suite*

The volcanic suite is characterized by the presence of numerous small, rounded, subvolcanic xenoliths. Various medium-grained clinopyroxenite xenoliths ($\leqslant$5 cm wide) are present in the nephelinites; they may contain minor amounts of apatite and nepheline. In the phonolites, most of the xenoliths (<5 mm across) consist of various associations of euhedral clinopyroxene, titanite and sanidine in a groundmass of nepheline, and apatite (mainly melteigites and nepheline-syenites). Ibhi (2000) and Ibhi *et al*. (2002) also report the presence of spinel-bearing and spinel-free olivine clinopyroxenites, interpreted as high-pressure cumulates from the primitive alkaline magmas from Saghro.

Carbonatite xenoliths are also present in some nephelinites; they have been described in detail by Ibhi *et al*. (2002). They are rounded, millimetre to centimetre in size, and show a reactional F-rich corona at the contact with the host nephelinite. The carbonatite mineral assemblage comprises low-Mg calcite, apatite, clinopyroxene, Ba-rich biotite and pyrochlore.

## Analytical methods

Major element mineral compositions were determined by electron microprobe (Cameca SX100 at the CAMPARIS unit of the University of Paris VI, France). The operating conditions were as follows: an accelerating voltage of 15 keV, a probe current of 10nA and a probe diameter of ~1 μm. For nosean, a 1 μm probe causes damage to the analysed surface and may enhance alkali diffusion and to avoid this problem the beam was defocused to ~5 μm in diameter. The counting time was fixed at 10 s for both peak and background measurements. The standards used were pure synthetic albite for Na, natural diopside for Mg, Si and Ca, natural orthoclase for K and Al, and oxides for Fe ($Fe_2O_3$), for Cr ($Cr_2O_3$) and for Mn and Ti, ($MnTiO_3$).

An additional microprobe session for the minor elements including F, Cl and S was performed at the CAMST (University of Louvain-la-Neuve, Belgium) on a Cameca SX50 microprobe. The counting times for minor elements was increased to 20 s. Standards for major elements were the same as those used in the CAMPARIS service. Reference materials for the minor elements and volatile analyses were a *REE*-rich synthetic glass for Ce, synthetic $ZrO_2$ for Zr, strontianite for Sr, baryte for Ba and S, Nb metal for Nb and apatite for P. Lithium fluoride and vanadinite were used for the calibration of F and Cl respectively. Detection limits for light elements (Si, Al, Mg, Ca, Na, K, F, Cl, S) are generally close to 0.03 wt.%. For the heavy elements and P, they vary within the ranges 0.07−0.10 and 0.05−0.24 wt.% respectively. Accuracy of the analyses is estimated as being close to ±1% for the major elements and ~±10% for the minor elements.

Whole-rock major elements were measured by ICP-AES at the Musée Royal de l'Afrique Centrale (Tervuren, Belgium). Before crushing the samples, all the parts showing traces of alteration were removed with a saw. Rock powders were digested by alkali fusion by heating a mix of 0.3 g of sample and 0.9 g of lithium metaborate (used as a flux) for 2 h at 1000ºC. The glasses were then diluted into a low-concentration $HNO_3$ solution before being analysed. The calibration was made using a combination of seven international rock standards.

## Mineral chemistry

### *Clinopyroxene*

In the nephelinites, the groundmass clinopyroxene is a diopside with a high Mg# (80−90) and low Al and Na contents (Fig. 5, Table 1), while the phenocrysts are Ti-augite (Fig. 5*a*, Table 1). The various types of nephelinites display no significant differences in pyroxene composition with the exception of the pyroxene nephelinites which display a wider range of compositions. The phenocrysts can be classified into three types: (1) augite with green core showing the lowest Mg# (43−67) and high Al and Na contents; (2) large crystals with a dark brown core made of high-Al augite (Mg#: 65−83; up to 0.44 Al a.p.f.u.; Fig. 5*c*) with high Ca/Na and Al/Ti ratios; (3) small euhedral phenocrysts with a composition (Mg#: 74−83; Al/Ti: 2−6) close to that of the groundmass pyroxene and similar to the light-brown mantle surrounding the core of the two previous phenocryst types. A detailed description of pyroxene compositions from a single pyroxene-nephelinite flow is given in Berger *et al*. (2008).

The phonotephrite clinopyroxenes show a similar wide range of compositions for both groundmass crystals and phenocrysts (Fig. 5*b*). The green aegirine-augite is Na-Fe-rich (Mg#: 37−53; Na: 0.10−0.20) whereas the brown augite is richer in magnesium (Mg#: 60−74).

The composition of pyroxenes in phonolites displays a continuous trend (Fig. 5*b*; Table 1), with groundmass aegirine-augite compositions partly overlapping those of the augite phenocrysts but with overall lower Mg#'s (25−65 *vs*. 35−95) and distinct bulk Ca/Na ratios (<5 *vs*. 15−70). Some green phenocrysts from TIM1 have a chemical composition close to that of the groundmass pyroxene, but locally are richer in Fe. A microprobe line scan (Fig. 6) through a green-and-brown clinopyroxene in contact with a nepheline-apatite-hainite-aegirine microdomain (Fig. 4*c*) shows a clearly bicompositional crystal with a strong enrichment in Na and Fe towards the rim − up to 0.53 and 0.76 a.p.f.u, respectively, with a Mg# as low as 17 close to the peralkaline assemblage. The groundmass clinopyroxene from the Si-rich phonolites is restricted to a nearly-pure aegirine composition with low contents in Mg and Al (<0.080 a.p.f.u.).

### *Olivine*

Olivine is present in the nephelinites, phonotephrites and in two phonolite flows. Its compositional range is rather restricted, varying from $Fo_{84}$−$Fo_{89}$ (Fig. 7; Table 1), with the exception of the olivine-phenocryst rims in sample TAF7, which are characterized by compositions significantly smaller in Fo ($Fo_{80-81}$) and greater in Ca (0.020−0.024 *vs*. 0.006−0.013 a.p.f.u. in other samples).

### *Nepheline*

In the nephelinites, this phase is only present as a groundmass mineral. Its composition (Table 2) is close to the ideal Buerger composition $KNa_3Al_4Si_4O_{16}$ (Hamilton, 1961), i.e. a low-vacancy site occupancy (<0.130 a.p.f.u.), a small excess silica (Qz% <0.26), a small Ca content (An% <0.86) and a K/Na ratio approaching 1/3 (from $Ne_{68}Ks_{32}$ to $Ne_{75}Ks_{25}$, Fig. 8). The melilite-olivine nephelinite is, however, characterized by a greater Ca content in nepheline (up to 4%).

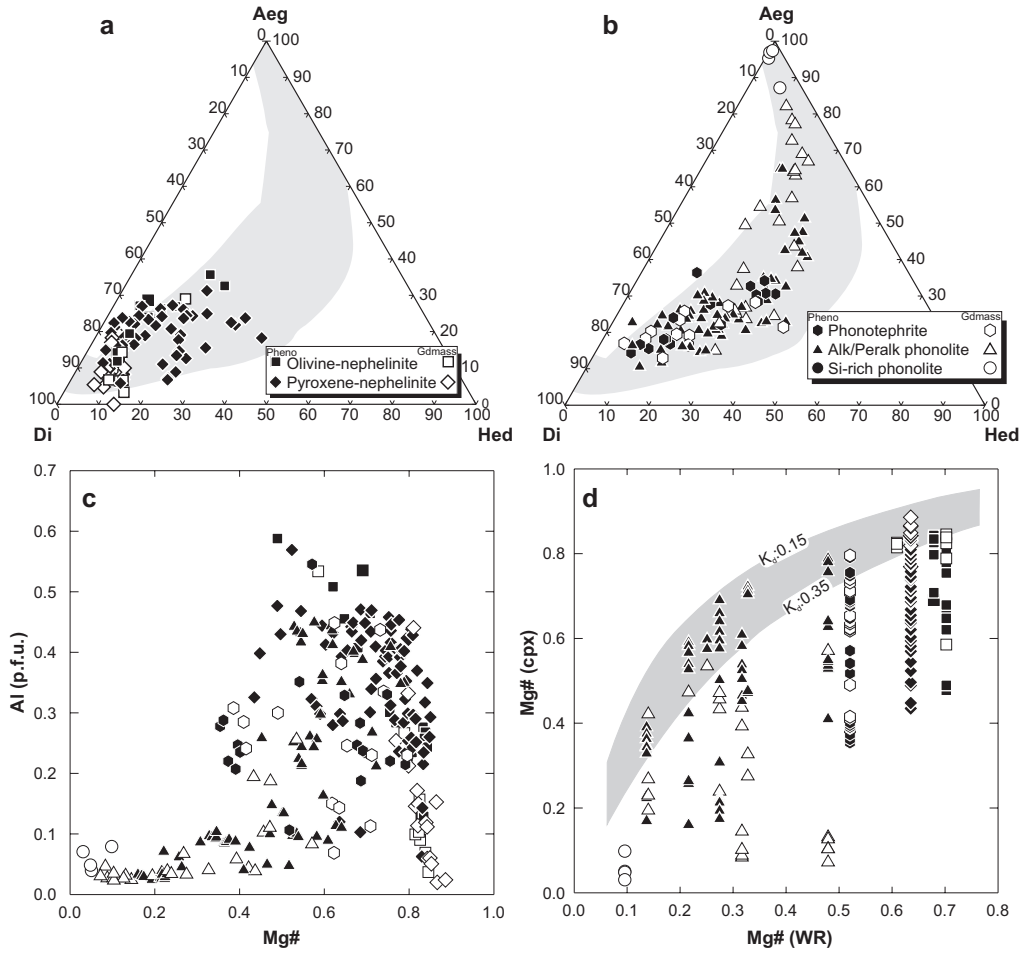


FIG. 5. Composition of the pyroxenes from Saghro. (*a*) and (*b*) Aegirine-diopside-hedenbergite diagrams for the nephelinites and the phonolites, respectively; the grey shaded areas show the composition of the pyroxenes from the Tamazeght complex (from Marks *et al*., 2008). (*c*) Mg# *vs*. Al content in clinopyroxene; note the large Al content of intermediate Mg#-pyroxenes. (*d*) Clinopyroxene *vs*. whole-rock Mg# diagram used to discriminate pyroxenes in equilibrium with their host lava. The equilibrium value is bracketed between 0.15 and 0.35.

The phonolites and the phonotephrite have a nepheline richer in Na, with K/Na ratios ranging from 0.10 to 0.28. Nepheline from the phonotephrite shows a large silica excess ($Ne_{73-79}Ks_{7-16}Qz_{7-15}$). The phonolites have nepheline phenocrysts with a small silica content ($Ne_{78-81}Ks_{12-20}Qz_{0-4}$) and their groundmass nepheline shows a greater silica excess ($Ne_{77-81}Ks_{12-15}Qz_{5-8}$). In both rock types, nepheline shows different types of habit (hexagonal and square sections), but there is no systematic compositional difference between the various morphological types. Some phenocrysts however show a strong compositional zoning (K/Na: 0.16 to 0.20 from core to rim).

The Si-rich phonolites also show a restricted range of composition for nepheline ($Ne_{77-80}K_{12-16}Qz_{5-10}$) except for the glomerocrysts that have a greater amount of Na ($Ne_{83}K_{12}Qz_5$).

### *Alkali feldspar*

The phonotephrite has a wide range of feldspar compositions (Table 2), from $Or_{48}$ to $Or_{71}$. In phonolite flows, this phase also shows a wide, but

TABLE 1. Representative analyses of olivine and clinopyroxene from Saghro lavas.

| Sample | FN 4 | FS 5 | TABS 7 | FS 10 | FN 4 | FS 10 | FS 5 | FN 4 | AS 1 | AS 1 | OUL 3 | TG 4 | AZLO-U 1 | TIM 1 | BAG 2 | BAG 2 | TG 4 | BAG 2 | MIG 2 | IK 07 |
|---|---|---|---|---|---|---|---|---|---|---|---|---|---|---|---|---|---|---|---|---|
| Host | Ol-neph | Px-neph | Si-poor Ph | Px-neph | Ol-neph | Px-neph | Px-neph | Ol-neph | Ph-tephrite | Ph-tephrite | Alkaline Ph | Peralk Ph | Peralk Ph | Peralk Ph | Peralk Ph | Peralk Ph | Peralk Ph | Peralk Ph | Peralk Ph | Si-rich Ph |
| Setting | Pheno-cryst | Pheno-cryst | Pheno-cryst | Pheno-cryst | Pheno-cryst | Pheno-cryst | Pheno-cryst | Ground-mass | Pheno-cryst | Pheno-cryst | Ground-mass | Pheno-cryst | Pheno-cryst | Pheno-cryst | Pheno-cryst | Pheno-cryst | Ground-mass | Ground-mass | Ground-mass | Ground-mass |
| Min | Olivine | Olivine | Olivine | Pyrox-ene | Pyrox-ene | Pyrox-ene | Pyrox-ene | Pyrox-ene | Pyrox-ene | Pyrox-ene | Pyrox-ene | Pyrox-ene | Pyrox-ene | Pyrox-ene | Pyrox-ene | Pyrox-ene | Pyrox-ene | Pyrox-ene | Pyrox-ene | Pyrox-ene |
| Type | | | | Dark core | Green core | Light mantle | Small unzoned | | Brown | Green core | Green | Green | Green | Green | Rim | Green | Green | Green | Green | Green |
| $SiO_2$ | 40.29 | 38.85 | 40.94 | 45.08 | 41.48 | 48.44 | 47.67 | 52.71 | 47.63 | 46.44 | 50.11 | 51.57 | 51.57 | 44.85 | 51.89 | 49.95 | 52.04 | 52.06 | 51.84 | 52.41 |
| $TiO_2$ | | | | 2.89 | 3.20 | 1.82 | 2.33 | 1.31 | 2.54 | 0.78 | 0.97 | 0.83 | 0.63 | 3.17 | 1.08 | 0.79 | 2.79 | 1.79 | 1.42 | 2.44 |
| $Al_2O_3$ | | | | 10.10 | 11.93 | 5.40 | 6.02 | 0.86 | 5.84 | 4.83 | 5.75 | 2.01 | 2.24 | 7.43 | 0.75 | 2.07 | 0.60 | 0.68 | 0.66 | 1.09 |
| $Cr_2O_3$ | | | | 0.32 | 0.00 | 0.00 | 0.12 | 0.03 | 0.23 | 0.00 | 0.04 | 0.00 | 0.04 | 0.00 | 0.00 | 0.00 | 0.05 | 0.00 | 0.12 | 0.03 |
| FeO | 11.70 | 15.74 | 11.06 | 5.06 | 10.74 | 6.82 | 6.26 | 4.99 | 6.73 | 18.34 | 16.78 | 11.75 | 15.30 | 9.40 | 21.95 | 18.48 | 24.60 | 23.31 | 22.57 | 25.31 |
| MnO | 0.13 | 0.31 | 0.19 | 0.11 | 0.09 | 0.11 | 0.07 | 0.14 | 0.15 | 0.90 | 0.83 | 0.66 | 1.18 | 0.16 | 0.88 | 1.07 | 0.58 | 0.72 | 0.76 | 1.00 |
| MgO | 46.95 | 43.76 | 47.26 | 12.31 | 8.51 | 13.27 | 13.76 | 15.30 | 13.55 | 5.72 | 4.23 | 10.26 | 7.65 | 10.21 | 3.65 | 5.47 | 1.56 | 2.67 | 3.05 | 0.72 |
| CaO | 0.29 | 0.33 | 0.34 | 22.82 | 22.40 | 23.19 | 23.92 | 23.93 | 22.69 | 20.26 | 15.41 | 21.10 | 18.23 | 23.24 | 10.74 | 16.58 | 6.51 | 7.47 | 8.28 | 1.55 |
| $Na_2O$ | | | | 0.61 | 0.87 | 0.61 | 0.56 | 0.67 | 0.54 | 2.10 | 4.36 | 1.93 | 3.32 | 0.96 | 7.59 | 4.34 | 9.97 | 9.26 | 8.30 | 13.27 |
| Total | 99.36 | 98.99 | 99.79 | 99.30 | 99.22 | 99.66 | 100.71 | 99.94 | 99.90 | 99.37 | 98.48 | 100.11 | 100.16 | 99.42 | 98.53 | 98.75 | 98.70 | 97.96 | 97.00 | 97.82 |
| Olivine formulae based on 4 oxygens, pyroxenes on 6 oxygens, $Fe^{3+}$ estimated by local charge balance | | | | | | | | | | | | | | | | | | | | |
| Si | 1.003 | 0.988 | 1.013 | 1.674 | 1.575 | 1.797 | 1.747 | 1.937 | 1.765 | 1.801 | 1.928 | 1.935 | 1.948 | 1.693 | 1.987 | 1.927 | 1.990 | 1.997 | 2.016 | 1.977 |
| $^{[4]}Al$ | | | | 0.326 | 0.425 | 0.203 | 0.253 | 0.037 | 0.235 | 0.199 | 0.072 | 0.065 | 0.052 | 0.307 | 0.013 | 0.073 | 0.010 | 0.003 | 0.000 | 0.023 |
| Ti | | | | 0.081 | 0.091 | 0.051 | 0.064 | 0.036 | 0.071 | 0.023 | 0.028 | 0.023 | 0.018 | 0.090 | 0.031 | 0.023 | 0.080 | 0.052 | 0.042 | 0.069 |
| $^{[6]}Al$ | | | | 0.116 | 0.108 | 0.034 | 0.007 | 0.000 | 0.020 | 0.022 | 0.189 | 0.024 | 0.048 | 0.023 | 0.021 | 0.021 | 0.017 | 0.028 | 0.030 | 0.025 |
| Cr | | | | 0.009 | 0.000 | 0.000 | 0.003 | 0.001 | 0.007 | 0.000 | 0.001 | 0.000 | 0.001 | 0.000 | 0.000 | 0.000 | 0.001 | 0.000 | 0.004 | 0.001 |
| $Fe^{3+}$ | | 0.021 | | 0.084 | 0.198 | 0.111 | 0.154 | 0.063 | 0.106 | 0.289 | 0.150 | 0.133 | 0.211 | 0.174 | 0.493 | 0.330 | 0.570 | 0.561 | 0.476 | 0.829 |
| $Fe^{2+}$ | 0.243 | 0.313 | 0.229 | 0.073 | 0.142 | 0.100 | 0.038 | 0.090 | 0.103 | 0.306 | 0.389 | 0.235 | 0.273 | 0.123 | 0.210 | 0.266 | 0.216 | 0.187 | 0.258 | 0.000 |
| Mn | 0.003 | 0.007 | 0.004 | 0.004 | 0.003 | 0.004 | 0.002 | 0.004 | 0.005 | 0.030 | 0.027 | 0.021 | 0.038 | 0.005 | 0.029 | 0.035 | 0.019 | 0.023 | 0.025 | 0.032 |
| Mg | 1.741 | 1.660 | 1.743 | 0.682 | 0.482 | 0.734 | 0.752 | 0.838 | 0.749 | 0.331 | 0.243 | 0.574 | 0.431 | 0.575 | 0.208 | 0.314 | 0.089 | 0.152 | 0.177 | 0.040 |
| Ca | 0.008 | 0.009 | 0.009 | 0.908 | 0.911 | 0.922 | 0.939 | 0.942 | 0.901 | 0.842 | 0.635 | 0.849 | 0.738 | 0.940 | 0.441 | 0.685 | 0.267 | 0.307 | 0.345 | 0.063 |
| Na | | | | 0.044 | 0.064 | 0.044 | 0.040 | 0.048 | 0.039 | 0.158 | 0.325 | 0.140 | 0.244 | 0.070 | 0.564 | 0.325 | 0.739 | 0.689 | 0.626 | 0.970 |
| Mg# | 87.7 | 84.1 | 88.4 | 81.3 | 58.6 | 77.6 | 79.7 | 84.5 | 78.2 | 35.7 | 31.0 | 60.9 | 47.1 | 65.9 | 22.9 | 34.5 | 10.1 | 16.9 | 19.4 | 4.8 |

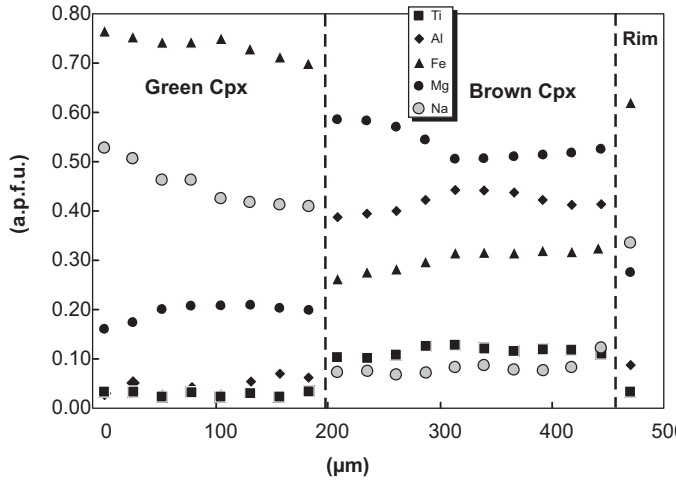


FIG. 6. Bicompositional brown and green pyroxene at the contact with a peralkaline hainite-bearing domain in a phonolite. See Fig. 4*c* for the precise location of this grain.

significantly distinct, range in Or content ($Or_{60-90}$), without any significant difference between the groundmass crystals and the phenocrysts in any given sample. The Si-rich phonolites have the most Na-rich feldspar ($Or_{40-57}$). Alkali feldspars display virtually no compositional zoning except in two samples: (1) a constant composition throughout the core of the crystals with a thin rim enriched in K (ELB6); (2) a progressive increase in K from the core towards

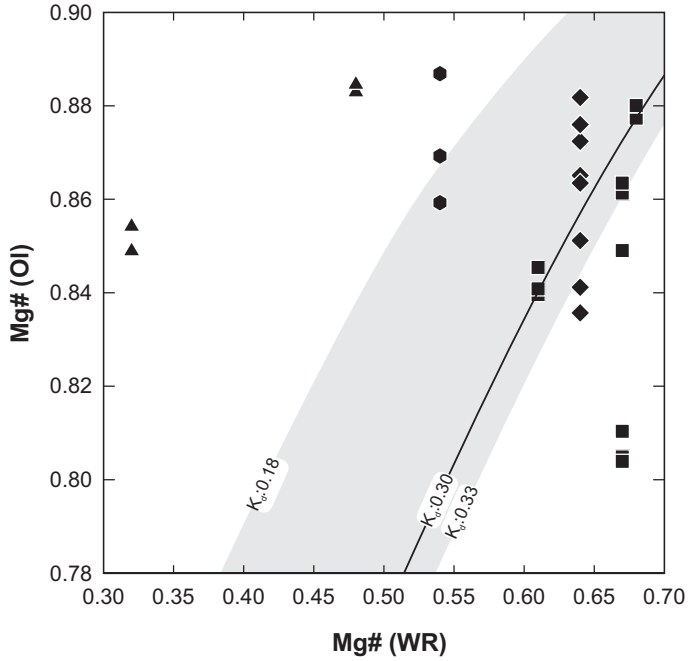


FIG. 7. Olivine compositions for the Saghro Cenozoic nephelinites/phonolites and theoretical field of olivine in equilibrium with host lava (from 0.18 to 0.33, see text). Symbols as in Fig. 5.

TABLE 2. Representative analyses of nephelines and feldspars.

| Sample | FS 17 | TL 4 | AS 1 | OUL 3 | OUL 3 | TG 4 | MIG 2 | AZLOU 1 | BAG 2 | IK 07 | IK 07 |
|---|---|---|---|---|---|---|---|---|---|---|---|
| Rock | Px-neph | Mel-neph | Ph-tephrite | Alkaline Ph | Alkaline Ph | Peralk Ph | Peralk Ph | Peralk Ph | Peralk Ph | Si-rich Ph | Si-rich Ph |
| Min | Nepheline | Nepheline | Nepheline | Nepheline | Nepheline | Nepheline | Nepheline | Nepheline | Nepheline | Nepheline | Nepheline |
| Type | Groundmass | Groundmass | Groundmass | Phenocryst | Groundmass | Phenocryst | Phenocryst | Groundmass | Groundmass | Phenocryst | Groundmass |
| $SiO_2$ | 40.91 | 41.25 | 49.49 | 42.78 | 45.70 | 43.29 | 46.20 | 46.23 | 45.60 | 47.69 | 46.77 |
| $Al_2O_3$ | 32.85 | 32.88 | 29.75 | 34.01 | 32.09 | 33.04 | 31.85 | 29.63 | 31.65 | 30.89 | 30.61 |
| FeO | 1.25 | 1.19 | 0.80 | 0.64 | 0.84 | 0.66 | 0.73 | 2.45 | 1.05 | 0.72 | 1.78 |
| MgO | 0.26 | 0.22 | 0.14 | | 0.05 | 0.03 | | 0.12 | 0.03 | | 0.03 |
| CaO | 0.12 | 0.86 | 0.08 | 0.87 | 0.55 | | | | 0.17 | | 0.04 |
| $Na_2O$ | 14.67 | 15.30 | 16.28 | 15.81 | 15.56 | 17.42 | 17.12 | 16.69 | 15.64 | 17.52 | 17.51 |
| $K_2O$ | 9.25 | | 3.25 | 5.97 | 5.22 | 5.36 | 3.95 | 4.16 | 4.47 | 2.95 | 3.40 |
| Sum | 99.31 | 99.70 | 99.79 | 100.08 | 100.01 | 99.80 | 99.85 | 99.28 | 98.61 | 99.77 | 100.14 |
| Formulae based on 32 oxygens | | | | | | | | | | | |
| Si | 8.097 | 8.107 | 9.287 | 8.232 | 8.706 | 8.348 | 8.769 | 8.913 | 8.771 | 9.004 | 8.882 |
| Al | 7.663 | 7.615 | 6.579 | 7.712 | 7.206 | 7.509 | 7.124 | 6.733 | 7.176 | 6.874 | 6.851 |
| Fe | 0.207 | 0.195 | 0.125 | 0.102 | 0.133 | 0.106 | 0.116 | 0.395 | 0.169 | 0.113 | 0.283 |
| Mg | 0.078 | 0.065 | 0.038 | | 0.013 | | | 0.035 | 0.008 | | 0.009 |
| Ca | 0.026 | 0.182 | 0.016 | 0.180 | 0.111 | 0.007 | | | 0.035 | | 0.007 |
| Na | 5.628 | 5.830 | 5.924 | 5.899 | 5.749 | 6.512 | 6.302 | 6.238 | 5.832 | 6.412 | 6.447 |
| K | 2.336 | 1.997 | 0.777 | 1.466 | 1.269 | 1.318 | 0.957 | 1.024 | 1.096 | 0.710 | 0.823 |
| Ne% | 70.1 | 71.2 | 74.1 | 75.6 | 73.1 | 80.5 | 78.6 | 77.1 | 74.3 | 79.5 | 79.8 |
| K% | 29.1 | 24.4 | 9.7 | 18.8 | 16.1 | 16.3 | 11.9 | 12.7 | 14.0 | 8.8 | 10.2 |
| An% | 0.6 | 4.4 | 0.4 | 4.6 | 2.8 | 0.2 | 0.0 | 0.0 | 0.9 | 0.1 | 0.2 |
| Q% | 0.2 | 0.0 | 15.8 | 0.9 | 7.9 | 3.0 | 9.4 | 10.2 | 10.9 | 11.5 | 9.8 |

| Sample | AS 1 | AS 6 | OUL 3 | TAB 7 | TIM 1 | BAG 2 | MIG 2 | TAB 7 | TIM 1 | ELB 6 | IK 07 |
|---|---|---|---|---|---|---|---|---|---|---|---|
| Rock | Ph-tephrite | Ph-tephrite | Alkaline Ph | Peralk Ph | Peralk Ph | Peralk Ph | Peralk Ph | Peralk Ph | Peralk Ph | Si-rich Ph | Si-rich Ph |
| Min | Feldspar | Feldspar | Feldspar | Feldspar | Feldspar | Feldspar | Feldspar | Feldspar | Feldspar | Feldspar | Feldspar |
| Type | Phenocryst | Phenocryst | Groundmass | Phenocryst | Phenocryst | Phenocryst | Groundmass | Groundmass | Groundmass | Phenocryst | Groundmass |
| $SiO_2$ | 65.06 | 65.11 | 65.88 | 65.85 | 65.70 | 64.93 | 65.56 | 64.83 | 65.35 | 66.66 | 65.52 |
| $Al_2O_3$ | 18.99 | 18.33 | 19.22 | 19.05 | 18.16 | 18.28 | 18.13 | 17.85 | 18.45 | 18.24 | 18.78 |
| FeO | 0.28 | 0.15 | 0.55 | 0.17 | 0.15 | 0.28 | 0.95 | 1.21 | 0.84 | 0.21 | 0.50 |
| MgO | | | | | | | | | 0.08 | | |
| CaO | 0.36 | | 0.34 | 0.09 | 0.06 | | | | | 0.10 | 0.04 |
| $Na_2O$ | 5.71 | 4.14 | 2.65 | 2.53 | 3.18 | 3.27 | 4.24 | 2.52 | 3.16 | 6.68 | 4.93 |
| $K_2O$ | 8.14 | 11.30 | 11.35 | 12.08 | 12.37 | 12.32 | 10.36 | 12.57 | 12.10 | 7.38 | 10.13 |
| SrO | | | | | | 0.14 | | | | | |
| BaO | | | | | | 0.64 | | | | | |
| Sum | 98.54 | 99.03 | 99.99 | 99.77 | 99.62 | 99.86 | 99.24 | 98.98 | 99.98 | 99.27 | 99.90 |
| Formulae based on 8 oxygens | | | | | | | | | | | |
| Si | 2.970 | 2.991 | 2.986 | 2.996 | 3.008 | 2.995 | 3.000 | 3.001 | 2.986 | 3.013 | 2.978 |
| Al | 1.022 | 0.993 | 1.027 | 1.022 | 0.980 | 0.994 | 0.978 | 0.974 | 0.993 | 0.971 | 1.006 |
| Fe | 0.011 | | 0.021 | 0.006 | 0.006 | 0.011 | 0.036 | 0.047 | 0.032 | 0.008 | 0.019 |
| Mg | | | | | | | | | 0.006 | | |
| Ca | 0.018 | 0.001 | 0.016 | 0.005 | 0.003 | | | | | 0.005 | 0.002 |
| Na | 0.505 | 0.368 | 0.233 | 0.223 | 0.282 | 0.293 | 0.376 | 0.226 | 0.280 | 0.585 | 0.434 |
| K | 0.474 | 0.662 | 0.656 | 0.701 | 0.723 | 0.725 | 0.605 | 0.742 | 0.705 | 0.425 | 0.587 |
| $X_{An}$ | 1.8 | 0.1 | 1.8 | 0.5 | 0.3 | 0.0 | 0.1 | 0.0 | 0.1 | 0.5 | 0.2 |
| $X_{Ab}$ | 50.7 | 35.7 | 25.8 | 24.0 | 28.0 | 28.8 | 38.3 | 23.4 | 28.4 | 57.6 | 42.4 |
| $X_{Or}$ | 47.5 | 64.2 | 72.4 | 75.5 | 71.7 | 71.2 | 61.6 | 76.6 | 71.5 | 41.9 | 57.4 |

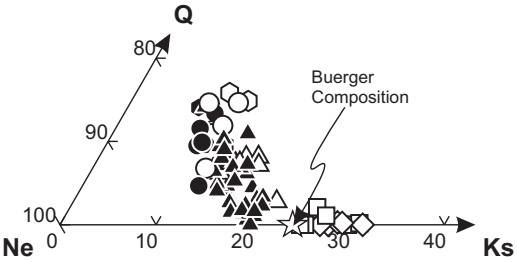


FIG. 8. Composition of the nephelines from Saghro in a molar Ne-Q-Ks diagram. Symbols as in Fig. 5.

the rim (TIM1: from $Or_{68}$ in the core to $Or_{73}$ at the rim). Ba and Sr contents are very small in most feldspars, except in sample BAG1 where SrO and BaO contents do reach 0.15 and 0.48 wt.%, respectively.

### *Fe-Ti oxides*

The Fe-Ti oxides in Saghro belong to the magnetite-ulvöspinel solid-solution series. They are Ti-magnetites $Uv_{48-70}Mag_{30-52}$ with large Mg contents (0.201−0.328 a.p.f.u.; Table 3). The phonolites show a restricted range in Ti-magnetite composition $Uv_{29-37}Mag_{63-71}$, with greater amounts of Mn compared to those of Ti-magnetite in nephelinites, but lesser Mg contents. The oxides from the phonotephrite have a compositional range that lies between those of phonolites and nephelinites ($Uv_{27-63}Mag_{37-73}$; Table 3).

### *Minor and accessory phases*

Apatite has a large F content compared to Cl (1.7−2.7 wt.% and <0.3 wt.% respectively) and also a large Sr content (1.7−3.3 SrO wt.%; Table 4). The *REE* content is small, as illustrated by the measured Ce concentrations (<0.7 $Ce_2O_3$ wt.%).

Feldspathoids of the nosean-sodalite group are present in phonolites and in the phonotephrite; the composition is that of virtually pure nosean ($SO_3$: 6−7 wt.%; Cl: 0.6−1 wt.%; Table 4).

The melilite (Table 4), found in only one nephelinite, is dominated by the Mg-åkermanite component (53 mol.%) with a significant amount of Na-melilite (33 mol.%) and Fe-akermanite (12 mol%).

Titanite is present in most phonolites; the sum of the oxides for the major elements is low (93−94 wt.%). *REE*s are present in the structure ($\leqslant$2 wt.% $Ce_2O_3$, Table 4), but this phase is also rich in $Nb_2O_5$ (1 wt.%); $ZrO_2$ (1 wt.%), SrO

TABLE 3. Representative analyses of Fe-Ti oxides.

| Sample | TAF 7 | FS 10 | FS 5 | AS 1 | AS 1 | TO 4 | MIG 2 | IK 07 |
|---|---|---|---|---|---|---|---|---|
| Rock Type | Ol-neph Ground-mass | Px-neph Ground-mass | Px-neph Ground-mass | Ph-tephrite Ground-mass | Ph-tephrite Ground-mass | Si-poor Ph Phenocryst | Peralk Ph Phenocryst | Si-rich Ph Phenocryst |
| $TiO_2$ | 19.47 | 12.24 | 11.79 | 18.67 | 6.03 | 8.43 | 9.92 | 9.61 |
| $Al_2O_3$ | 1.17 | 0.10 | 0.48 | 0.48 | 0.33 | 0.41 | 1.28 | 0.38 |
| $Cr_2O_3$ | 0.41 | 0.20 | 0.28 | 0.13 | | | 0.07 | |
| FeO | 67.60 | 74.75 | 72.79 | 69.40 | 82.95 | 82.86 | 78.95 | 79.85 |
| MnO | 1.19 | 1.38 | 1.34 | 1.57 | 1.20 | 2.11 | 2.11 | 2.13 |
| MgO | 5.10 | 3.57 | 5.56 | 2.61 | 1.60 | 0.06 | 0.51 | 0.11 |
| Sum | 94.94 | 92.24 | 92.24 | 92.86 | 92.11 | 93.87 | 92.84 | 92.08 |
| Formulae based on 3 cations, $Fe^{3+}$ estimated by charge balance | | | | | | | | |
| Ti | 0.536 | 0.351 | 0.330 | 0.534 | 0.175 | 0.244 | 0.289 | 0.283 |
| Al | 0.050 | 0.004 | 0.021 | 0.021 | 0.015 | 0.019 | 0.058 | 0.018 |
| $Fe^{3+}$ | 0.898 | 1.306 | 1.354 | 0.974 | 1.640 | 1.498 | 1.363 | 1.428 |
| Cr | 0.012 | 0.006 | 0.008 | 0.004 | 0.000 | 0.000 | 0.002 | 0.002 |
| $Fe^{2+}$ | 1.172 | 1.077 | 0.913 | 1.234 | 1.036 | 1.165 | 1.190 | 1.185 |
| Mn | 0.037 | 0.044 | 0.042 | 0.051 | 0.039 | 0.069 | 0.069 | 0.071 |
| Mg | 0.279 | 0.203 | 0.309 | 0.148 | 0.092 | 0.003 | 0.029 | 0.007 |

TABLE 4. Representative analyses of accessory minerals.

| Mineral | Apatite | Apatite | Apatite | Melilite | Del hayelite | Del hayelite | Nosean | Nosean | Sphene | Sphene | Perovs-kite | Perovs-kite |
|---|---|---|---|---|---|---|---|---|---|---|---|---|
| Sample | FS 17 | TL 6 | TIM 1 | TL 6 | BAG 2 | BAG 2 | AS 6 | TABS 7 | TABS 7 | MIG 2 | FS 5 | FS 17 |
| Rock | Px-neph | Mel-neph | Si-poor Ph | Mel-neph | Si-poor Ph | Si-poor Ph | Ph-teph | Si-poor Ph | Si-poor Ph | Peralk Ph | Px-neph | Px-neph |
| Type | Ground mass | Ground mass | Ground mass | Ground mass | Ground mass | Ground mass | Pheno-cryst | Pheno-cryst | Pheno-cryst | Pheno-cryst | Ground mass | Ground mass |
| $P_2O_5$ | 40.03 | 40.92 | 40.13 | | | | | | | | | |
| $Nb_2O_5$ | | | | | | | | | 0.60 | 0.47 | 2.00 | 1.41 |
| $SiO_2$ | 0.95 | 1.18 | 0.74 | 42.79 | 55.09 | 55.21 | 35.17 | 36.21 | 30.03 | 30.02 | 0.30 | 0.25 |
| $TiO_2$ | 0.08 | 0.17 | | 0.12 | 0.14 | 0.00 | 0.00 | 0.00 | 36.28 | 36.20 | 50.99 | 51.20 |
| $ZrO_2$ | | | | | | | | | 0.38 | 0.82 | | |
| $Al_2O_3$ | 0.00 | 0.03 | | 6.57 | 6.26 | 6.27 | 31.23 | 30.88 | 1.18 | 1.17 | 0.10 | 0.17 |
| $Ce_2O_3$ | | | 0.20 | | | | | | 0.22 | | 2.37 | 2.93 |
| FeO | 0.17 | 0.25 | | 2.87 | 0.53 | 0.35 | 0.11 | 0.15 | 1.29 | 1.52 | 1.17 | 1.30 |
| MgO | 0.00 | 0.06 | | 7.75 | | | | | | | | |
| CaO | 52.74 | 53.81 | 52.88 | 33.67 | 16.56 | 16.62 | 1.71 | 1.03 | 28.08 | 27.51 | 32.65 | 32.87 |
| SrO | 3.32 | 1.79 | 2.05 | 1.59 | 0.54 | 0.57 | 0.37 | 0.13 | 0.08 | 0.07 | 1.10 | 0.84 |
| BaO | 0.62 | 0.22 | | 0.30 | | | | | | | | |
| $Na_2O$ | 0.00 | 0.00 | 0.18 | 3.45 | 7.24 | 7.98 | 19.93 | 19.85 | 0.10 | 0.10 | 1.04 | 0.92 |
| $K_2O$ | 0.00 | 0.05 | 0.02 | 0.16 | 6.08 | 6.21 | 1.75 | 1.16 | | 0.05 | | |
| $SO_2$ | 0.11 | 0.05 | 0.29 | | 0.16 | 0.19 | 7.27 | 7.96 | 0.05 | | | |
| F | 2.30 | 1.71 | 2.69 | | 1.69 | 1.78 | 0.04 | | 0.10 | 0.11 | | |
| Cl | 0.03 | 0.21 | | | 1.47 | 1.54 | 1.01 | 0.67 | | | | |
| Subtotal | 100.36 | 100.44 | 99.18 | 99.25 | 95.76 | 96.71 | 98.60 | 98.04 | 98.40 | 98.02 | 91.71 | 91.89 |
| Less O≡F,Cl | 0.97 | 0.77 | 1.13 | 0.00 | 1.04 | 1.09 | 0.25 | 0.15 | 0.04 | 0.05 | 0.00 | 0.00 |
| Sum | 99.38 | 99.67 | 98.04 | 99.25 | 94.71 | 95.62 | 98.35 | 97.88 | 98.36 | 97.98 | 91.71 | 91.89 |

| Mineral | Hainite | Hainite | Hainite | Loren-zenite | Amphi-bole | Amphi-bole | Biotite | Biotite | Biotite | Eud-group | Eud-group |
|---|---|---|---|---|---|---|---|---|---|---|---|
| Sample | TIM 1 | TIM 1 | BAG 2 | MIG 2 | AZLOU 1 | AZLOU 1 | TL 6 | FS 17 | AS 1 | MIG 2 | MIG 2 |
| Rock | Si-poor Ph | Si-poor Ph | Si-poor Ph | Peralk Ph | Si-poor Ph | Si-poor Ph | Mel-neph | Px-neph | Ph-teph | Peralk Ph | Peralk Ph |
| Type | Ground mass | Ground mass | Ground mass | Titanite rim | Pheno-cryst | Pheno-cryst | Ground mass | Ground mass | Ground mass | Titanite rim | Titanite rim |
| $P_2O_5$ | 0.14 | 0.14 | 0.19 | | | 0.07 | | | | | 0.07 |
| $Nb_2O_5$ | 1.17 | 1.03 | 1.43 | 0.95 | | | | | | 0.82 | 0.67 |
| $SiO_2$ | 31.31 | 31.37 | 31.19 | 34.46 | 38.02 | 38.34 | 24.34 | 26.26 | 35.75 | 53.38 | 54.90 |
| $TiO_2$ | 8.98 | 9.27 | 9.62 | 44.08 | 5.69 | 5.21 | 11.25 | 9.52 | 6.09 | 6.96 | 7.10 |
| $ZrO_2$ | 4.41 | 4.16 | 0.31 | 0.12 | | | | 0.16 | | 1.95 | 3.03 |
| $Al_2O_3$ | 0.03 | | | 0.11 | 13.22 | 13.19 | 16.18 | 13.59 | 15.14 | 0.06 | 0.04 |
| $Ce_2O_3$ | 1.23 | 1.27 | 2.11 | | | | | 0.19 | | | |
| FeO | 0.59 | 0.55 | 0.33 | 0.77 | 10.31 | 10.31 | 8.97 | 6.09 | 8.26 | 4.00 | 4.35 |
| MgO | 0.04 | 0.04 | | | 12.36 | 12.61 | 10.78 | 13.58 | 17.26 | 0.03 | 0.02 |
| CaO | 34.91 | 35.03 | 37.07 | 0.31 | 11.82 | 11.90 | 0.07 | 0.57 | 0.07 | 9.48 | 9.87 |
| SrO | 0.88 | 0.88 | 0.91 | | 0.15 | 0.15 | | | | 0.60 | 0.58 |
| BaO | | | 0.12 | | 0.12 | 0.37 | 20.93 | 18.54 | 1.10 | | 0.22 |
| $Na_2O$ | 6.51 | 6.49 | 6.26 | 17.27 | 2.16 | 2.09 | 0.13 | 0.18 | 0.89 | 7.97 | 5.23 |
| $K_2O$ | | | 0.24 | 0.03 | 2.15 | 2.22 | 2.38 | 2.54 | 8.74 | 0.35 | 0.25 |
| $SO_2$ | | | | | | | | | | 0.18 | 0.22 |
| F | 4.29 | 4.35 | 4.58 | | 0.08 | 0.09 | 0.43 | 1.18 | 0.33 | | 0.03 |
| Cl | | 0.02 | | | | | | | | 1.11 | 1.14 |
| Subtotal | 94.48 | 94.58 | 94.35 | 98.09 | 96.08 | 96.56 | 95.46 | 92.38 | 93.63 | 86.87 | 87.71 |
| Less O≡F,Cl | 1.81 | 1.83 | 1.93 | 0.00 | 0.03 | 0.04 | 0.18 | 0.50 | 0.14 | 0.25 | 0.27 |
| Sum | 92.67 | 92.75 | 92.42 | 98.09 | 96.04 | 96.52 | 95.28 | 91.88 | 93.49 | 86.62 | 87.44 |

(1 wt.%) and F (1.5 wt.%). Even when including these components, the sum of the oxides remains small, which may be ascribed to the presence of other unmeasured *REE* (especially *MREE*) and other minor elements such as Ta and Hf.

Biotite in the nephelinites has an unusual composition; it is Ba-rich (up to 21 wt.% BaO, = 1.335 Ba a.p.f.u..), but is also rich in Ti (9−12 $TiO_2$ wt.%). A few biotite grains have also been identified in the phonotephrite; they show a lower Mg# (75 instead of 85 in the nephelinites).

The amphibole from Saghro is a kaersutite (Table 4) with an Mg# ranging from 83 to 88. It shows trace amounts of SrO and BaO (0.15 and 0.12−0.37 wt.% respectively).

Hainite ($Na_4Ca_8(Ti,Zr,Mn,Fe)_3Si_8O_{28}F_8$) from Saghro is the first occurrence reported in Morocco. This mineral has been described in a syenite from Poços de Caldeira, Brazil (Atencio *et al*., 1999) and in Bohemia, Czech Republic; (Ulrych *et al*., 1992). It is a Na-Ca-K-Ti fluoro-sorosilicate (4 wt.% F) that contains large amounts of some elements usually present only in trace quantities (Table 4): $\leqslant$2.8 wt.% $Ce_2O_3$, 1.8 wt.% $Nb_2O_5$, 4 wt.% $ZrO_2$ and $\leqslant$1.1 wt.% SrO. The sum of the oxides is relatively low, possibly due to the presence of hydroxyl radicals and/or to undetermined large quantities of Ta, Hf and *REE*s (Atencio *et al*., 1999).

Lorenzenite ($Na_2Ti_2Si_2O_9$), from sample MIG1, is close to the pure end-member composition (Table 4), but nevertheless shows significant amounts of Fe, Ca and Nb (0.9−1.2 wt.% $Nb_2O_5$).

Perovskite is rich in *REE* ($Ce_2O_3$ in the range 2.3−2.9 wt.%), Sr (>1 wt.% SrO), Nb ($\leqslant$2 wt.% $Nb_2O_5$) and Na ($\leqslant$2 wt.% $Na_2O$). Here again, all the minor elements have not been analysed and the contents of Ta and other *REE*s are probably high, as is frequently the case in perovskite from nephelinites (Platz *et al*., 2004).

One silicate phase surrounding lorenzenite has not been clearly identified. Its low sum of oxides (86−87 wt.%) probably indicates the presence of water and/or hydroxyl radicals. The large silica content together with the presence of Na and Ti is a common feature of the eudialyte-group minerals, which are common in magmatic peralkaline systems.

A water-rich mineral ($(Na,K)_{10}Ca_5Al_6Si_{32}O_{80}(Cl_2,F_2,SO_4)_3.18(H_2O)$), first described in nephelinites from northern Kivu in Congo (Sahama and Kai Hytonen, 1959), has also been identified in association with hainite. The mineral has the same Si/Al ratio as delhayelite, but is significantly richer in K and Ca. Such features are observed in the delhayelite-rhodesite-macdonaldite family.

## Whole-rock major-element data

A selection of representative rock samples have been analysed to determine their major element compositions (Table 5). The nephelinites have low silica (37−40 wt.% $SiO_2$) and rather high alkali contents (4−6 wt.% $Na_2O+K_2O$) for ultrabasic lavas. One pyroxene-nephelinite (TAB3) is slightly more differentiated (42.8 wt.% $SiO_2$; $Na_2O+K_2O$: 7.6 wt.%). As expected, the phonolites display greater alkali (13−16 wt.%) and silica contents (50−56 wt.%), the phonolites cropping out as domes being the most Si-rich (55−56 wt.% $SiO_2$). The lavas from Saghro are among the most Si-undersaturated and alkali-rich Cenozoic volcanic rocks in Morocco and the Canary Islands (Fig. 9*a*; Lustrino and Wilson, 2007 and references therein). Unlike the Siroua stratovolcano located 200 km to the west (Berrahma and Delaloye, 1989), the Saghro lavas do not show both Si-undersaturated and Si-saturated trends. The peralkaline index is above unity for most phonolites (Fig. 9*b*) except for two phonolite flows and one sample from a phonolite dome. Si-rich samples have a lower peralkaline index than the mean value of less-differentiated phonolites, which suggests fractionation of alkali-rich cumulates (agpaites?) during the last steps of differentiation.

In terms of major element oxides *vs*. whole-rock Mg# (Fig. 10), three trends can be distinguished. (1) The Ti, Fe, Mg, Ca, and P contents are high in nephelinites (MgO: 8−14 wt.%; CaO: 11−16 wt.%), they decrease strongly towards high Mg# phonolites then more gently in the peralkaline and Si-rich phonolite field. (2) The Al, Na and K contents are small in the nephelinites ($Al_2O_3$: 10−12 wt.%) then increase strongly towards more mafic phonolites. The Al content is similar for most phonolite types (19−22 $Al_2O_3$ wt.%) but is least (~20 wt.%) in the most Si-rich phonolites. The Na and K contents are quite variable in phonolites (6−11 wt.% $Na_2O$; 4−8 wt.% $K_2O$) but the most differentiated phonolites generally have a lesser mean alkali content than other phonolites (except for non-peralkaline samples). (3) The Si content increases gradually from nephelinites to phonolites but the trend is steeper from nephelinites to phonolites than between the mafic and the more differentiated phonolites.

TABLE 5. Whole-rock major element data for the Saghro Cenozoic lavas.

| Sample | TAF 7 | FN 4 | TL 6 | FS 5 | TAB 3 | AS 1 | OUL 3 | TO 1 | TAB 1 | TG 1 | AZLOU 1 | TIM 1 | SAR 3 | BAG 2 | MIG 2 | TAB 7 | IK 01 | ELB 6 |
|---|---|---|---|---|---|---|---|---|---|---|---|---|---|---|---|---|---|---|
| Rock type | Ol-neph | Ol-neph | Ol-mel neph | Px-neph | Px-neph | Ph-te-phrite | Alka-line Ph | Alka-line Ph | Peralk Ph | Peralk Ph | Peralk Ph | Peralk Ph | Peralk Ph | Peralk Ph | Peralk Ph | Peralk Ph | Si-rich Ph | Si-rich Ph |
| $SiO_2$ | 37.24 | 39.30 | 39.02 | 39.68 | 42.75 | 47.75 | 50.27 | 52.42 | 49.99 | 52.20 | 52.58 | 52.80 | 54.40 | 54.30 | 54.92 | 54.38 | 54.65 | 55.51 |
| $Al_2O_3$ | 11.83 | 10.67 | 10.84 | 11.37 | 13.61 | 16.42 | 21.30 | 21.53 | 19.21 | 19.77 | 19.56 | 20.68 | 19.90 | 20.95 | 20.69 | 20.37 | 20.16 | 20.81 |
| $Fe_2O_3$ tot | 12.75 | 11.72 | 12.35 | 11.71 | 10.64 | 7.46 | 3.85 | 4.47 | 4.80 | 5.22 | 4.99 | 4.08 | 4.27 | 3.62 | 3.76 | 3.59 | 3.78 | 2.89 |
| MnO | 0.23 | 0.19 | 0.18 | 0.21 | 0.18 | 0.19 | 0.14 | 0.15 | 0.17 | 0.20 | 0.22 | 0.18 | 0.24 | 0.19 | 0.22 | 0.20 | 0.22 | 0.21 |
| MgO | 10.04 | 13.96 | 13.18 | 10.30 | 8.40 | 4.76 | 0.65 | 0.58 | 2.44 | 1.25 | 1.23 | 0.78 | 0.39 | 0.29 | 0.31 | 0.15 | 0.20 | 0.34 |
| CaO | 14.51 | 13.32 | 14.35 | 15.37 | 10.98 | 7.92 | 3.74 | 2.53 | 4.63 | 3.09 | 2.91 | 2.67 | 1.77 | 1.78 | 1.36 | 1.10 | 0.88 | 0.89 |
| $Na_2O$ | 3.81 | 3.41 | 2.80 | 3.06 | 4.45 | 6.19 | 5.70 | 7.86 | 8.33 | 9.42 | 10.38 | 8.93 | 9.08 | 9.63 | 10.60 | 9.22 | 8.86 | 9.83 |
| $K_2O$ | 2.06 | 1.94 | 1.31 | 1.73 | 3.15 | 4.03 | 7.71 | 7.69 | 6.06 | 6.10 | 5.13 | 6.52 | 6.71 | 6.61 | 5.65 | 6.95 | 4.54 | 5.09 |
| $TiO_2$ | 3.48 | 2.76 | 2.93 | 2.76 | 2.80 | 1.81 | 0.68 | 0.89 | 0.98 | 0.90 | 0.91 | 0.71 | 0.47 | 0.48 | 0.49 | 0.32 | 0.36 | 0.25 |
| $P_2O_5$ | 2.05 | 1.16 | 1.76 | 1.64 | 0.88 | 0.58 | 0.06 | 0.12 | 0.17 | 0.21 | 0.22 | 0.09 | 0.02 | 0.06 | 0.03 | 0.31 | 0.00 | 0.00 |
| LOI | 1.19 | 1.84 | 1.42 | 2.67 | 1.19 | 2.06 | 6.88 | 2.25 | 2.15 | 1.21 | 0.70 | 1.21 | 2.15 | 1.52 | 0.80 | 3.34 | 5.12 | 3.65 |
| Sum | 99.20 | 100.26 | 100.16 | 100.50 | 99.03 | 99.18 | 100.99 | 100.50 | 98.93 | 99.58 | 98.83 | 98.65 | 99.39 | 99.44 | 98.82 | 99.94 | 98.77 | 99.44 |

## Discussion

### *Fractional crystallization: mineralogical arguments and modelling of the major element data.*

The Saghro alkaline volcanic suite is characterized by the paucity of rocks with intermediate composition between nephelinites and phonolites. This is classically referred to as the Daly gap (Daly, 1910; Baker, 1968). One may thus ask whether these two groups of rocks are cogenetic or have different modes of formation. Two main arguments – clinopyroxene composition and fractional crystallization modelling – suggest that intermediate lavas probably exist at depth but have not been erupted at the surface.

The variation of clinopyroxene composition is continuous from nephelinites to phonolites in the Saghro series, i.e. the Mg# varies from 85 to 0 without compositional gap; continuous variations are also observed for the Ca/Na and Al/Ti ratios. Clinopyroxene phenocrysts in nephelinites have a Mg# varying from 85 to 40 or, in terms of Fe-Mg clinopyroxene/whole rock ratio (hereafter Fe-Mg Cpx/WR ratio) between 0.15 and 0.35. Considering a mean of 0.27 (Damasceno *et al.*, 2002), the clinopyroxenes with Mg# between 75 and 55 are in equilibrium with melts having Mg# ranging between 30 and 50, which is just the Mg# gap between the nephelinites and most phonolites. The continuous clinopyroxene compositional range observed in the nephelinites also argues for the existence of intermediate lithologies at depth in the Saghro area.

To test whether fractional crystallization is a suitable mechanism to link the nephelinites to the phonolites, modelling using the mass-balance law was performed using the whole-rock major element data and the composition of the main mineral phases measured using the electron microprobe. The first step of the modelling was to select the most appropriate parental melt. The olivine-melilite nephelinite TL-6 was a good candidate because it has a small phenocryst content and is characterized by a large Mg# (68) and small Si, Na and K contents. The olivine-nephelinite FN4 has a greater Mg# than TL-6 but the phenocryst proportion is large (10 vol.% Ol; 18 vol.% Cpx) meaning that the whole-rock composition probably does not represent the composition of a liquid. From the parental melt TL6, a theoretical trend made of seven steps of differentiation (corresponding to Mg# values of 65, 60, 50, 40, 30, 20, 10) was arbitrarily chosen to fit the natural whole-rock data. Then, the

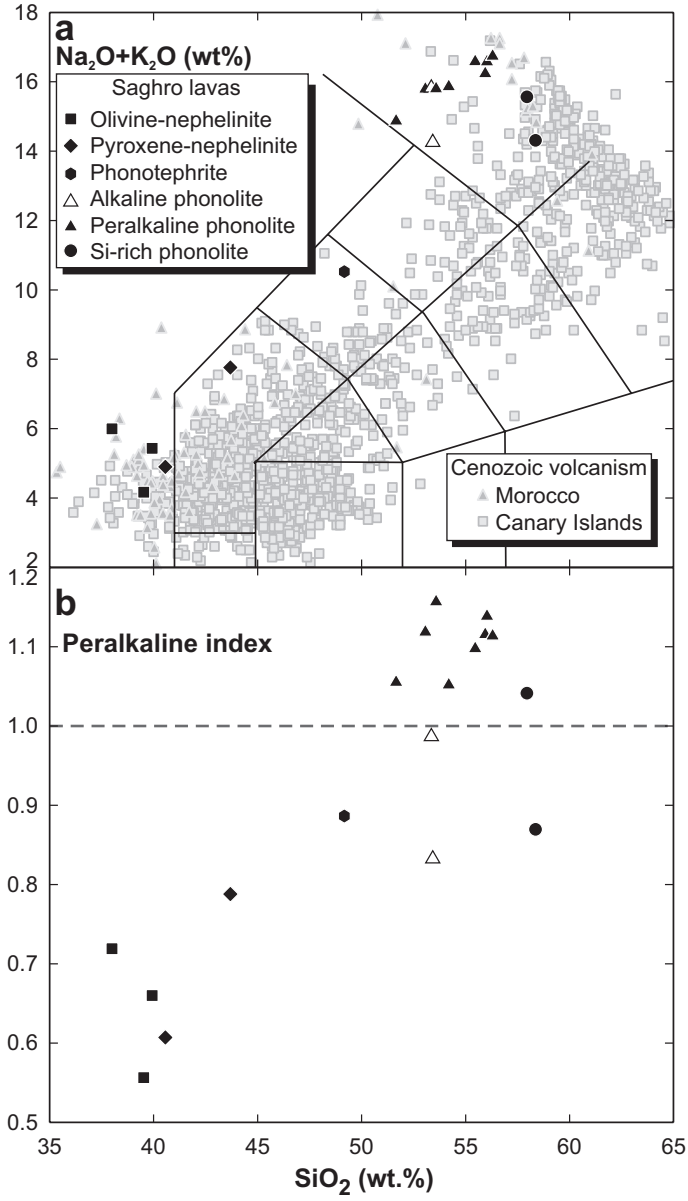


FIG. 9. (*a*) TAS diagram showing the composition of the Saghro lavas compared to those of the Cenozoic volcanic rocks from Morocco and Canary Islands (from Lustrino and Wilson, 2007). (*b*) Variation of the peralkaline index with silica content. The analyses were normalized to 100% on a $H_2O$ and $CO_2$-free basis, for nomenclature purposes.

evolution from the parental melt to the first theoretical differentiated melt was calculated by subtracting a theoretical cumulate. The same approach was used for the seven steps. The variables are the rate of fractionation (the fraction of the mass of cumulate extracted at each step) and the modal proportions of the successive cumulates. The compositions used for the mineral solid-solutions are those measured by electron microprobe for phenocrysts that were in equilibrium with each theoretical melt composition. For clinopyroxene, a diopside-augite was

used for the nephelinites and an aegirine-augite for peralkaline phonolites. The quality of the modelling at each step was controlled with the value of the residue between the theoretical melt and the melt obtained by subtracting the cumulate belonging to the melt composition of the preceding step. If the sum of the squares of the residue for each major element oxide is small (<1), it means that the theoretical model fits well to the natural data. Values of the unknown variables were adjusted automatically by successive iterations. Some samples however do not represent true liquid composition because they have large phenocryst contents. The theoretical trend (Fig. 10) thus follows the natural trend that corresponds to both nearly aphyric samples (<10 vol.% phenocrysts) and porphyritic lavas.

The squares of the residues vary from 0.08 to 0.68 for the first six steps of the modelling and are slightly greater than 1 (1.28) but still acceptable for the seventh and final step. The modal proportions of the seven computed cumulates are presented in Fig. 11 and Table 6 while their major-element composition is plotted in Fig. 10.

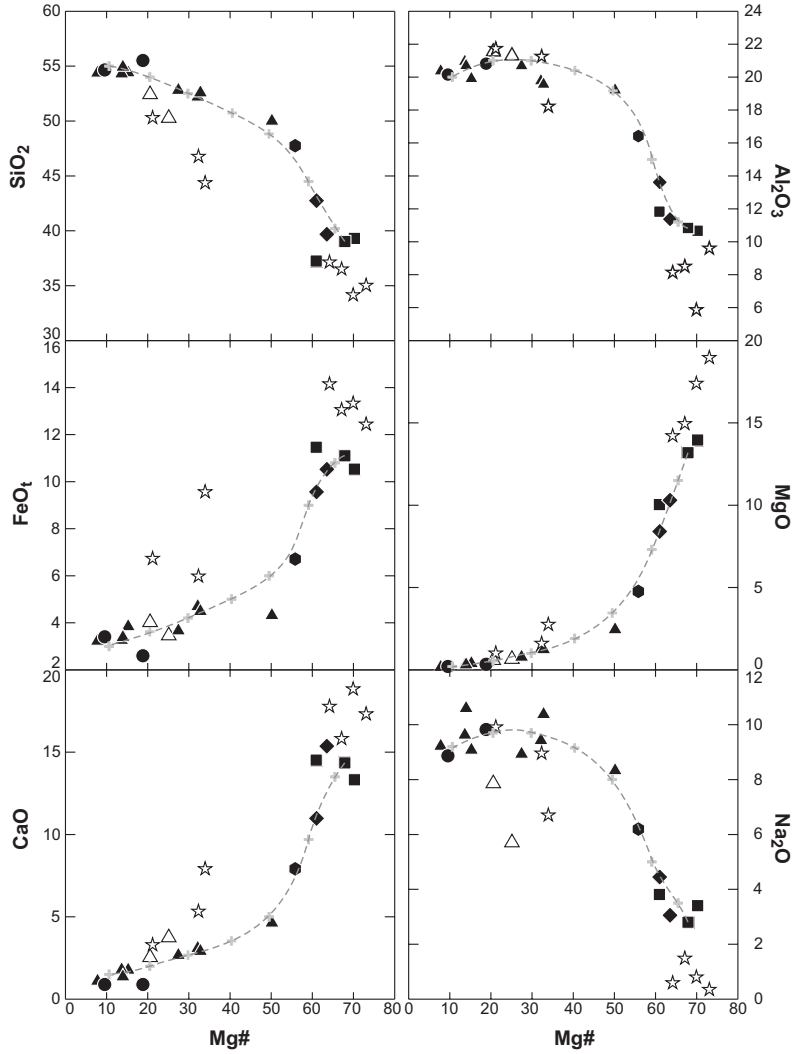


FIG. 10. Whole-rock Mg# *vs*. major-element oxide (wt.%) variation diagrams for the Saghro lavas. The crosses represent the composition of the successive theoretical lavas modelled by fractional crystallization (see text for discussion) and the stars represent the composition of computed cumulates. Symbols as in Fig. 9.

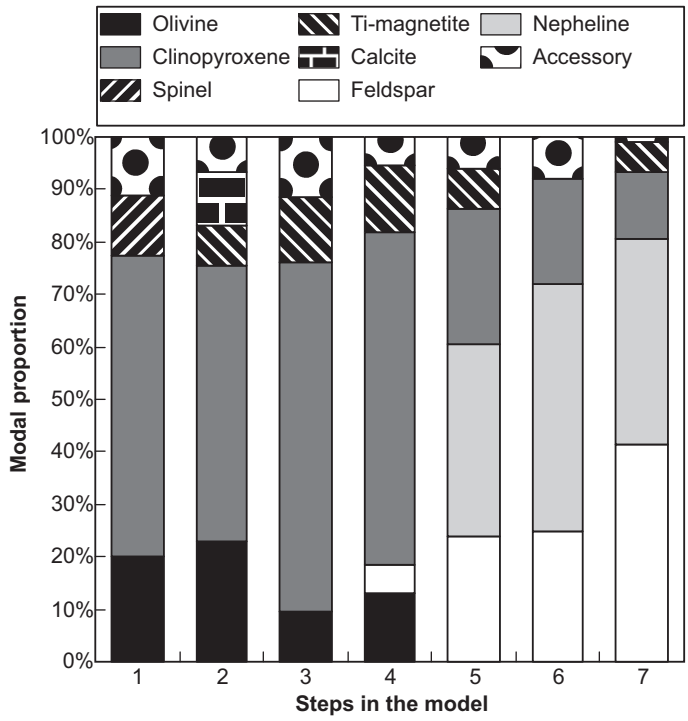


FIG. 11. Modal proportion of the seven cumulates computed in the fractional-crystallization model. Accessory minerals correspond to Ti-magnetite, apatite, calcite, titanite, spinel, biotite, amphibole and nosean.

Cumulates fractionated during the first four steps are mainly olivine-clinopyroxenites (plutonic rocks dominated by clinopyroxene and olivine) with various accessory minerals. The most primitive cumulate contains ~10% of aluminous spinel and accessory apatite (4 wt.%) and Ti-magnetite (4 wt.%). For the first and second steps, the best fit (lowest residues) between the calculated and the observed trends is obtained by subtracting a calcite-bearing cumulate, with 2% calcite in step 1 and 4% in step 2. This suggests that carbonate is a cumulate or immiscible phase in the Saghro alkaline series. In the Saghro lavas, the calcite is found as carbonatite xenoliths (with pyrochlore and apatite; Ibhi *et al*., 2002); in the groundmass of some nephelinites, it is found in a fine-grained assemblage with clinopyroxene, apatite and Ba-rich biotite and also as small inclusions in olivine phenocrysts. The absence of carbonate globules or immiscibility-generated textures within Saghro lavas and the purely calcic content of the carbonate phases seems to suggest that calcite was not formed by immiscibility during crystallization of the nephelinite melt. Crystallization of calcite from a carbonated nephelinite magma has been proved experimentally (Lee and Wyllie, 1998) and has been observed in other similar magmatic systems (Verhulst *et al*., 2000; see Mitchell, 2005). Moreover, in Saghro, the carbonatite xenoliths belong to a suite of xenolithic rocks comprising wehrlites, pyroxenites and nepheline-syenites which are undoubtedly formed by fractional crystallization of the nephelinite-phonolite lava suite. Further geochemical investigations using Nb/Ta ratios in the Saghro nephelinite-phonolite lavas (work in progress) will bring more constraints on the choice between immiscibility and fractional crystallization for the origin of the calcite phase.

The association of accessory phases changes slightly from step to step: it consists of Ti-magnetite (4%) + Ca carbonate (3%) + apatite (3%) + nepheline (1%) for step 1 and to Ti-magnetite (8%) + apatite (4%) + biotite (3%) + amphibole (4%) for step 2**.** From step 5, nepheline and alkali feldspar are the dominant fractionating phases (from 5 to 47 wt.% and from 5 to 41%

TABLE 6. Modal composition of the modelled cumulates and the fractionation rate and sum of the squares of residues for each step.

| Phases | Ol | Cpx | Fsp | Ne | Ti-mag | Spl | Ttn | Bt | Amph | Ap | Cc | No | Fractionation rate (R) | $\Sigma R^2$ | Composition of ol, cpx and ne in the cumulate | | |
|---|---|---|---|---|---|---|---|---|---|---|---|---|---|---|---|---|---|
| | Modal proportion (expressed as wt.%) | | | | | | | | | | | | | | Ol (Mg#) | Cpx (Mg#) | Ne |
| Steps | | | | | | | | | | | | | | | | | |
| 1 | 20.1 | 57.4 | | | 4.2 | 11.3 | | | | 4.1 | 2.9 | | 0.22 | 0.31 | 88.0 | 80 | |
| 2 | 23.1 | 52.3 | | 1.7 | 7.9 | 1.9 | | | | 3.0 | 10.1 | | 0.41 | 0.61 | 86.0 | 75 | $Ne_{70}Ks_{30}Q_0$ |
| 3 | 9.5 | 66.6 | 0.9 | | 12.5 | | | 2.6 | 4.2 | 3.6 | | | 0.37 | 0.46 | 84.0 | 73 | |
| 4 | 12.5 | 61.0 | 5.3 | 4.2 | 12.0 | | | | 0.5 | 4.5 | | | 0.10 | 0.08 | 81.0 | 69 | $Ne_{76}Ks_{24}Q_0$ |
| 5 | | 25.7 | 24.0 | 36.7 | 7.5 | | 4.0 | | | 2.2 | | | 0.20 | 0.27 | | 59 | $Ne_{80}Ks_{15}Q_5$ |
| 6 | | 20.0 | 24.9 | 47.3 | 3.4 | | 0.1 | | | 1.4 | | 2.9 | 0.21 | 0.19 | | 54 | $Ne_{80}Ks_{15}Q_5$ |
| 7 | | 12.7 | 41.5 | 39.2 | 5.7 | | 0.3 | | | 0.6 | | | 0.21 | 1.28 | | 50 | $Ne_{82}Ks_{12}Q_6$ |

respectively) and the modal proportion of clinopyroxene is decreasing (from 60 to 13 wt.%) while olivine ceases to fractionate. Cumulates of the last three steps are pyroxene-bearing nepheline syenites and malignites (step 5). The main accessory phases are titanite (from 4 to 1 wt.%), apatite (5–1 wt.%) and nosean (3 wt.% at step 6). Plutonic xenoliths observed in the Saghro lavas have broadly the same range of composition as the computed cumulates.

The modal proportions of the Saghro computed cumulates are similar to those observed in plutonic alkaline silicate massifs associated with carbonatites. An evolution from pyroxene-dominated cumulates (wehrlites and clinopyroxenites) to nepheline syenites (including malignites) is reported in the alkaline intrusions of the Kola peninsula (Downes *et al*., 2005 and references therein), Tamazeght (Marks *et al*., 2008 and references therein) and the Canary Islands (Munoz *et al*., 2005). It thus appears that fractional crystallization is a viable mechanism to link nephelinites to phonolites despite the paucity of lavas of intermediate composition. The latter are predicted by the modelling and their absence at the surface is most probably due to the high viscosity of intermediate magmas that can be related to their chemical composition and to the large total crystal contents (Richet *et al*., 1996; Thompson *et al*., 2001).

### *Origin of xenocrysts: nephelinite-phonolite mixing*

The Fe-Mg distribution coefficient ($K_{dFe\text{-}Mg}^{Mn/liq}$) between olivine or clinopyroxene and melt, together with petrographic observations can be used to test whether these minerals are in equilibrium with their host lava. Some lavas from Saghro probably do not represent true liquids because of the presence of large amounts of phenocrysts. In phonolites, the accumulation of alkali feldspar or nepheline does not change the bulk Fe/Mg ratio as these minerals are Fe- and Mg-poor. In nephelinites, pyroxenes and olivine are the dominant phenocrysts. The subtraction of the total phenocryst component from the nephelinite whole rock composition changes the Mg# of the sample only slightly, from 70 to 65 for sample FN4 and from 63 to 60 for sample FS5. This does not change the interpretations.

Most olivines from nephelinites are, on the basis of petrographical observations, in equilibrium with their host lava. Accordingly, they show Fe-Mg Ol/WR ratios ranging from 0.24 to

0.35, in the range of experimental $K_{dFe\text{-}Mg}^{Ol/liq}$ values (0.18−0.33, Gee and Sack, 1988; Ulmer, 1989; Fig. 7). However, the rims of olivine from the melilite-olivine nephelinite have greater ratios (0.49−0.51), suggesting that they are not in equilibrium with the host lava. These rims were probably enriched in iron during late-magmatic evolution. Resorbed olivines from phonolites are clearly out of equilibrium with their host lava (see petrographic description) and this is confirmed by the values of the Fe-Mg Ol/WR ratio (0.12−0.21).

A recent compilation has shown that the $K_{dFe\text{-}Mg}^{Cpx/liq}$ varies from 0.10 to 0.49 for a wide range of bulk compositions and that it strongly depends on crystallization temperature (Putirka *et al*., 2003). A mean of 0.27±0.07 is however generally accepted in studies concerning alkali basalts (Damasceno *et al*., 2002). The range of $K_{dFe\text{-}Mg}^{Cpx/liq}$ for phonolitic melts is not well constrained but a recent experimental study at low to moderate pressures shows that it varies from 0.07 to 0.44 (Freise *et al*., 2003), with most values around 0.19.

The groundmass clinopyroxenes from nephelinites have Fe-Mg Cpx/WR ratios close to, or within, the range considered at equilibrium (0.20−0.40). Among the different phenocryst types, only the small euhedral low-Al augites are in chemical equilibrium with the host lava (Fe-Mg Cpx/WR ratio: 0.30−0.37; Fig. 5*d*). Phenocrysts showing textural features such as sector zoning, resorption and corrosion gulfs (high-Al augite and green-core pyroxene) are clearly out of equilibrium and possess Fe-Mg Cpx/WR ratios in the range 0.45 to 2.89. Both phenocrysts and groundmass clinopyroxenes from the phonotephrite are not in equilibrium with the host lava (Fe-Mg Cpx/WR ratio: 0.35−2.25).

The compositions of both olivine and clinopyroxene indicate that the nephelinite and phonolite melts have interacted at depth. Indeed, nephelinites have clinopyroxene phenocrysts with green cores that are in equilibrium with phonolitic melts, while phonolites have olivine grains in equilibrium with a nephelinite magma. These interactions were already pointed out by Berger *et al*. (2008) who showed that, on the basis of the crystal size distribution and mineralogical arguments, some nephelinites have incorporated high-pressure (1 GPa) Na-Fe rich clinopyroxene phenocrysts which originally crystallized from a phonolitic melt. Such crystals are thus xenocrysts instead of phenocrysts: they could derive from a homogeneous chemical mixing or from a mechanical mingling of the two magmas. This can occur either during replenishment of a pre-existing phonolitic magma chamber with a mantle-derived nephelinite or by the existence of a compositionally-stratified nephelinitic/phonolitic magma chamber at lower crustal levels. However, as the xenocrysts are present in small proportions in both lava types (Berger *et al*., 2008), these interactions have probably only slightly modified the whole-rock composition of the lavas.

The only sampled phonotephrite shows phenocrysts that are not in equilibrium with the host bulk composition (Figs 5*d* and 7); it shows resorbed alkali feldspar, nosean, nepheline and amphibole phenocrysts. This sample is also remarkable in that it contains small volcanic xenoliths (former magma droplets?) of nephelinite composition. It thus represents a true mechanical mix between a phonolite melt carrying nepheline and nosean and a nephelinite melt carrying olivine and clinopyroxene.

### *Late magmatic crystallization and exchange*

Many interstitial microdomains are found between the alkali feldspar laths in the Saghro phonolites. They comprise nepheline, Sr-rich fluoroapatite, sanidine, aegirine and accessory minerals such as hainite and delhayelite. As already stated, hainite is an uncommon mineral described in Poços de Caldas, Brazil by Atencio *et al*. (1999) and Bohemia by Ulrych *et al*. (1992). It has not previously been identified in Morocco, but when present in other occurrences, it is always present as a late-crystallizing phase in peralkaline rocks. Delhayelite is present as a late-crystallizing groundmass phase in peralkaline silicate lavas associated with carbonatites at Oldoinyo Lengai, Tanzania (Dawson and Hill, 1998) and in Pian di Celle, Italy (Stoppa *et al*., 1997). At the contact with these interstitial domains, the brown augite phenocrysts are transformed into green aegirine-augite with a composition that matches that of groundmass pyroxene. Aegirine and aegirine-augite found as groundmass phases in the phonolites are also too Na- and Fe-rich to be in chemical equilibrium with their respective bulk lava compositions. Such textural and mineralogical features are rare in evolved alkaline lavas, but common in plutonic syenites (Wolff, 1987; Sørensen, 1997). Interstitial domains between the cumulus alkali feldspar and nepheline are generally enriched in alkalis, volatiles (F, Cl)

and minor and trace elements. The presence of strongly-alkaline intercumulus glass rich in Na, F, Zr has been observed in syenites from the Canary Islands (Wolff and Toney, 1993). Pockets of intercumulus holocrystalline material composed of låvenite, sodalite, loparite, perovskite, apatite (and many other *REE* and HFSE minerals) have been noted in many peralkaline syenites (Wolff, 1987; Moreau *et al*., 1996; Sørensen, 1997; Ridolfi *et al*., 2006). Similar assemblages are also described in subvolcanic dykes related to the Ilimaussaq intrusion (Marks and Markl, 2003). In the Saghro phonolites, the presence of alkali- and rare element-rich interstitial microdomains with hainite, apatite, nepheline, aegirine and rare sanidine and the 'aegirinization' of augitic phenocrysts close to these microdomains, points to a microscale fractional crystallization in the Saghro phonolites as in plutonic syenites. The crystallization of the main groundmass and phenocryst phases has led to the formation of a strongly-alkaline interstitial residual melt from which crystallized the assemblage described above. Exchange reactions between this evolved melt and surrounding pre-existing pyroxenes induced the formation of aegirine-augite as a replacement product of augite. The groundmass pyroxene from the phonolites is also too Na- and Fe-rich to be in equilibrium with the phonolite bulk-composition (Fig. 5*d*). It is however close in composition to the 'aegirinized' augite. It is thus suggested that, unlike some phenocrysts, the phonolite groundmass pyroxene is a late-stage crystallization product of the residual alkaline melt or the result of an exchange reaction between the residual melt and pre-existing groundmass augite. Thus, the combination of late, probably peralkaline, residual melts with a low solidus temperature would enhance crystallization of uncommon minerals that are normally found in agpaitic syenites. The late resorption of titanite in some peralkaline phonolites and its transformation into lorenzenite can be ascribed either to a late-magmatic reaction of the type described above, or to interaction of titanite with late, immiscible or hydrothermal Na-rich fluids. Such late- to post-magmatic reactions are also commonly observed in agpaitic syenites where primary peralkaline mineral associations are replaced by assemblages of silicates rich in Na, Ti, Zr and volatiles during multi-stage reactions with late-evolved melt or fluids (Coulson, 1997; Sørensen, 1997; Schmitt *et al*., 2002; Mitchell and Liferovich, 2006).

## Conclusions

The nephelinites and peralkaline phonolites (associated with a few carbonatites) from Saghro in southern Morocco form an exceptional suite of Mio-Pliocene alkaline lavas, among the most Si-undersaturated and alkali-rich of the whole West African Cenozoic volcanic province (including the Canary Islands).

Despite the lack of intermediate lavas at the surface, mineralogical arguments and major-element modelling show that the nephelinites and phonolites are linked by a fractional crystallization process. It implies the fractionation of cumulates dominated by olivine and clinopyroxene (with accessory Al-spinel/Ti-magnetite, ± apatite, calcite, biotite and amphibole) during the early stages and later by alkali feldspar and nepheline. These cumulates are comparable to the clinopyroxenites and nepheline syenites that constitute the main rock types of the plutonic ultramafic, alkaline and carbonatite complexes throughout the world. Such a plutonic complex is thus probably present under the Saghro volcanic province. The modelling also proves that carbonate-bearing rocks can be formed by fractional crystallization of a nephelinite magma.

Late-stage magmatic evolutions has led to the formation of minerals such as hainite, lorenzenite, delhayelite (and an eudialyte-group mineral) that are classically found in agpaitic syenites. Their formation results from the late-stage magmatic crystallization of residual melts or from late- to post-magmatic transformation of pre-existing phenocrysts. Such minerals are rarely observed in volcanic rocks (they are quite common in plutonic agpaitic syenites) but are of crucial importance to understanding the geochemical behaviour of rare elements (*REE*, Zr, Hf, Nb, Ta, F, Cl) in these magmatic systems.

Mixing is demonstrated by the presence of rare phonotephrites that are heterogeneous and contain minerals and xenoliths from both phonolitic and nephelinitic magmas. There is no evidence for the formation of an homogeneous mixed magma, probably because the two main melts (nephelinite and phonolite) have viscosities which are too different to enable mixing to take place.

## Acknowledgements

Jacques Wautier (CAMST-UCL) worked many days processing raw data from a complex microprobe session and checking for all inter-

ferences between major- and minor element X-ray peaks. Fieldwork by J.B. was supported by the ULB-Fonds Cambier in addition to the main Action 2 grant from the Belgian Federal Research Ministry. J.B. and N.E. acknowledge the local people of Saghro for their hospitality and help in the field, especially Amho for its translation from Berber into Arab and for guiding us through the Saghro Mountains. The constructive and helpful reviews of Michael Marks and Ray MacDonald are much appreciated; they contributed to significant improvements of the paper.

## References

Atencio, D., Coutinho, J.M.V., Ulbrich, M.N.C., Vlach, S.R.F., Rastsvetaeva, R.K. and Pushcharovsky, D.Y. (1999) Hainite from Poços de Caldas, Minas Gerais, Brazil. *The Canadian Mineralogist*, **37**, 91–98.

Baker, I. (1968) Intermediate oceanic volcanic rocks and the 'Daly gap'. *Earth and Planetary Science Letters*, **4**, 103–106.

Berger, J., Ennih, N., Liégeois, J-P., Nkono, C., Mercier, J-C. C. and Demaiffe, D. (2008) A complex multi-chamber magmatic system beneath a late Cenozoic volcanic field: evidence from CSDs and thermobarometry of clinopyroxene from a single nephelinite flow (Djbel Saghro, Morocco). Pp. 505–520 in: *The Boundaries of the West African Craton* (N. Ennih and J-P. Liégeois, editors). Special Publications, **297,** Geological Society of London.

Berrahma, M. and Delaloye, M. (1989) New geochronological data on the volcanic massif of Siroua (Anti-Atlas, Morocco). *Journal of African Earth Sciences*, **9**, 651–656.

Berrahma, M., Delaloye, M., Faure-Muret, A. and Rachdi, H.E.N. (1993) Premières données géochronologiques sur le volcanisme alcalin du Jbel Saghro, Anti-Atlas, Maroc. *Journal of African Earth Sciences*, **17**, 333–341.

Coulson, I.M. (1997) Post-magmatic alteration in eudialyte from the North Qoroq centre, South Greenland. *Mineralogical Magazine*, **61**, 99–109.

Currie, K.L., Eby, G.N. and Gittins, J. (1986) The petrology of the Mt. Saint Hilaire complex, southern Quebec: an alkaline gabbro-peralkaline syenite association. *Lithos*, **19**, 67–83.

Daly, R.A. (1910) The origin of alkaline rocks. *Science*, **32**, 220.

Damasceno, D., Scoates, J.S., Weis, D., Frey, F.A. and Giret, A. (2002) Mineral chemistry of mildly alkalic basalts from the 25 Ma Mont Crozier section, Kerguelen archipelago: Constraints on phenocryst crystallization environments. *Journal of Petrology*, **43**, 1389–1413.

Dawson, J.B. and Hill, P.G. (1998) Mineral chemistry of a peralkaline combeite-lamprophyllite nephelinite from Oldoinyo Lengai, Tanzania. *Mineralogical Magazine*, **62**, 179–196.

de Sitter, L.U., de Sitter-Koomans, C.M. and Heetveld, H. (1952) Les phonolites du Jebel Saghro (Maroc occidental). *Geologie en Mijnbouw*, **8**, 267–276.

Downes, H., Balaganskaya, E., Beard, A., Liferovich, R. and Demaiffe, D. (2005) Petrogenetic processes in the ultramafic, alkaline and carbonatitic magmatism in the Kola alkaline province: a review. *Lithos*, **85,** 48–75.

Freise, M., Holtz, F., Koepke, J., Scoates, J. and Leyrit, H. (2003) Experimental constraints on the storage conditions of phonolites from the Kerguelen archipelago. *Contributions to Mineralogy and Petrology*, **145**, 659–672.

Gee, L.L. and Sack, R.O. (1988) Experimental petrology of melilite nephelinites. *Journal of Petrology*, **29**, 1233–1255.

Hamilton, D.L. (1961) Nephelines as crystallisation temperature indicators. *Journal of Geology*, **69**, 321–329.

Ibhi, A. (2000) *Le volcanisme Plio-Quaternaire de Saghro (Anti-Atlas, Maroc) et les enclaves basiques et ultrabasiques associées*. PhD thesis, University of Agadir, Morocco, 354 pp.

Ibhi, A., Nachit, H., Abia, E.H. and Hernandez, J. (2002) Intervention des ségrégats carbonatitiques dans la pétrogenèse des néphélinites à pyroxène de Jbel Saghro (Anti-Atlas, Maroc). *Bulletin de la Sociéte Géologique de France*, **173**, 37–43.

Kogarko, L.N. and Romanchev, B.P. (1977) Temperature, pressure, redox conditions and mineral equilibria in agpaitic nepheline syenites and apatite-nepheline rocks. *Geochemistry International*, **14**, 113–128.

Kogarko, L.N., Kononova, V.A., Orlova, M.P. and Woolley, A.R. (1995) *Alkaline Rocks and Carbonatites of the World: Part 2, Former USSR.* Chapman and Hall, London, 225 pp.

Larsen, L.M. and Sørensen, H. (1987) The Ilimaussaq intrusion: progressive crystallization and formation of layering in an agpaitic magma. Pp. 473–488 in: *Alkaline Igneous Rocks* (J.G. Fitton and B.G.J. Upton, editors). Special Publications, **30,** Geological Society of London.

Lee, W.J. and Wyllie, P.J. (1998) Processes of crustal carbonatite formation by liquid immiscibility and differentiation, elucidated by model systems. *Journal of Petrology*, **39**, 2005–2013.

Liégeois, J-P., Benhallou, A., Azzouni-Sekkal, A., Yahiaoui, R. and Bonin, B. (2005) The Hoggar swell and volcanism: Reactivation of the Precambrian Tuareg shield during Alpine convergence and West African Cenozoic volcanism. Pp. 379–400 in: *Plates, Plumes and Paradigms* (G.R.

Foulger, J.H. Natland, D.C. Presnall and D.L. Anderson, editors). Special Paper **388**, Geological Society of America.

Lustrino, M. and Wilson, M. (2007) The circum-Mediterranean anorogenic Cenozoic igneous province. *Earth Science Reviews*, **81**, 1–65.

Malusa, M.G., Polino, R., Feroni, A.C., Ellero, A., Ottria, G., Baidder, L. and Musumeci, G. (2007) Post-variscan tectonics in eastern Anti-Atlas (Morocco). *Terra Nova*, **19**, 481–489.

Marks, M. and Markl, G. (2003) Ilimaussaq 'en miniature': closed-system fractionation in an agpaitic dyke rock from the Gardar province, South Greenland (contribution to the mineralogy of Ilimaussaq no. 117). *Mineralogical Magazine*, **67**, 893–919.

Marks, M.A.W., Schilling, J., Coulson, I.M., Wenzel, T. and Markl, G. (2008) The alkaline-peralkaline Tamazeght complex, High Atlas mountains, Morocco: Mineral chemistry and petrological constraints for derivation from a compositionally heterogeneous mantle source. *Journal of Petrology*, **49**, 1097–1131.

Mitchell, R.H. (2005) Carbonatites and carbonatites and carbonatites. *The Canadian Mineralogist*, **43**, 2049–2068.

Mitchell, R.H. and Liferovich, R.P. (2006) Subsolidus deuteric/hydrothermal alteration of eudialyte in lujavrite from the Pilansberg alkaline complex, South Africa. *Lithos*, **91**, 352–372.

Moreau, C., Ohnenstetter, D., Demaiffe, D. and Robineau, B. (1996) The Los archipelago nepheline syenite ring-structure: A magmatic marker of the evolution of the central and equatorial Atlantic. *The Canadian Mineralogist*, **34**, 281–299.

Munoz, M., Sagredo, J., de Ignacio, C., Fernandez-Suarez, J. and Jeffries, T.E. (2005) New data (U-Pb, K-Ar) on the geochronology of the alkaline-carbonatitic association of Fuerteventura, Canary Islands, Spain. *Lithos*, **85**, 140–153.

Platz, T., Foley, S.F. and Andre, L. (2004) Low-pressure fractionation of the Nyiragongo volcanic rocks, Virunga province, DR Congo. *Journal of Volcanology and Geothermal Research*, **136**, 269–295.

Putirka, K.D., Mikaelian, H., Ryerson, F. and Shaw, H. (2003) New clinopyroxene-liquid thermobarometers for mafic, evolved, and volatile-bearing lava compositions, with applications to lavas from Tibet and the Snake river plain, Idaho. *American Mineralogist*, **88**, 1542–1554.

Richet, P., Lejeune, A.M., Holtz, F. and Roux, J. (1996) Water and the viscosity of andesite melts. *Chemical Geology*, **128**, 185–197.

Ridolfi, F., Renzulli, A., Macdonald, R. and Upton, B.G.J. (2006) Peralkaline syenite autoliths from Kilombe volcano, Kenya rift valley: Evidence for subvolcanic interaction with carbonatitic fluids. *Lithos*, **91**, 373–392.

Sahama, T.G. and Kai Hytönen, M.A. (1959) Delhayelite, a new silicate from the Belgian Congo *Mineralogical Magazine*, **32**, 6–9.

Schmitt, A.K., Trumbull, R.B., Dulski, P. and Emmermann, R. (2002) Zr-Nb-REE mineralization in peralkaline granites from the Amis complex, Brandberg (Namibia): Evidence for magmatic pre-enrichment from melt inclusions. *Economic Geology*, **97**, 399–413.

Schonenberger, J., Marks, M., Wagner, T. and Markl, G. (2006) Fluid-rock interaction in autoliths of agpaitic nepheline syenites in the Ilimaussaq intrusion, South Greenland. *Lithos*, **91**, 331–351.

Sørensen, H. (1997) The agpaitic rocks – an overview. *Mineralogical Magazine*, **61**, 485–498.

Stoppa, F., Sharygin, V.V. and Cundari, A. (1997) New mineral data from the kamafugite-carbonatite association: The melilitolite from Pian di Celle, Italy. *Mineralogy and Petrology*, **61**, 27–45.

Tesón, E. and Teixell, A. (2008) Sequence of thrusting and syntectonic sedimentation in the eastern Sub-Atlas thrust belt (Dadès and Mgoun valleys, Morocco). *International Journal of Earth Sciences*, **97**, 103–113.

Thompson, G.M., Smith, I.E.M. and Malpas, J.G. (2001) Origin of oceanic phonolites by crystal fractionation and the problem of the Daly gap: An example from Rarotonga. *Contributions to Mineralogy and Petrology*, **142**, 336–346.

Ulbrich, H.H., Vlach., S.R.F., Demaiffe, D. and Ulbrich, M.N.C. (2005) Structure and origin of the Poços de Caldas alkaline massif, S.E. Brazil. Pp. 367–418 in: *Mesozoic to Cenozoic alkaline magmatism in the Brazilian platform* (P. Comin-Chiaramonti and C.B. Gomez, editors). Edit. de Universidade Sao Paulo, Brazil.

Ulmer, P. (1989) The dependence of the $Fe^{2+}$-Mg cation-partitioning between olivine and basaltic liquid on pressure, temperature and composition – an experimental study to 30 kbars. *Contributions to Mineralogy and Petrology*, **101**, 261–273.

Ulrych, J., Pivec, E., Rychly R. and Rutsek, J. (1992). Zirconium mineralization of young alkaline volcanic rocks from northern Bohemia. *Geologica Carpathica*, **43**, 91–95.

Verhulst, A., Balaganskaya, E., Kirnarsky, Y. and Demaiffe, D. (2000) Petrological and geochemical (trace elements and Sr-Nd isotopes) characteristics of the Paleozoic Kovdor ultramafic, alkaline and carbonatite intrusion (Kola peninsula, NW Russia). *Lithos*, **51**, 1–25.

Wolff, J.A. (1987) Crystallization of nepheline syenite in a subvolcanic magma system: Tenerife, Canary

Islands. *Lithos*, **20**, 207–223.
Wolff, J.A. and Toney, J.B. (1993) Trapped liquid from a nepheline syenite – a reevaluation of Na-rich, Zr-rich, F-rich interstitial glass in a xenolith from Tenerife, Canary Islands. *Lithos*, **29**, 285–293.